Controls on the morphology of closely spaced submarine canyons incising the continental slope of the northern South China Sea

Jian Li [a], Wei Li [a, b, *], Tiago M. Alves [c], Michele Rebesco[d], Xiujuan Wang[e], Shuang Li [a, b], Jie Sun [a], Wenhuan Zhan [a, b]

[a] Key Laboratory of Ocean and Marginal Sea Geology, South China Sea Institute of Oceanology, Innovation Academy of South China Sea Ecology and Environmental Engineering, Chinese Academy of Sciences, Guangzhou 511458, China

[b] University of Chinese Academy of Sciences, Beijing 100049, P.R. China

[c] 3D Seismic Lab. School of Earth and Ocean Sciences, Cardiff University, Main Building, Park Place, Cardiff, CF10 3AT, United Kingdom

[d] Istituto Nazionale di Oceanografia e di Geofisica Sperimentale (OGS), Borgo Grotta Gigante 42/C, Sgonico, 34010 Trieste, Italy

[e] Key Lab of Submarine Geosciences and Prospecting Techniques, MOE, Institute for Advanced Ocean Study, College of Marine Geosciences, Ocean University of China, Qingdao 266100, China

*Corresponding author: Dr. Wei Li (wli@scsio.ac.cn)

Highlights

- The morphology of submarine canyons changes gradually along a continental slope.

- High sediment supply and frequent sediment flows promote canyon erosion.

- Canyons to the southwest act as preferential pathways for sediment transportation.

- Seafloor scarps form physical barriers for sediment transported downslope.

Abstract

Submarine canyons are key elements in source-to-sink systems that are commonly developed along continental margins. They act as major conduits transferring sediment and pollutants from continental shelves to deep-water basins, and control the general morphology and evolution of continental margins. This work uses multibeam bathymetric and high-resolution (two- and three-dimensional) seismic data to investigate the main factors controlling the morphology of the Shenhu Canyon System in the northern South China Sea, as well as its detailed morphological character. The Shenhu Canyon System consists of nineteen (19) submarine canyons whose morphologies vary from southwest to northeast along the continental slope. Canyons (C1-C10) in the southwest show greater incision depths, and steeper thalwegs and walls, when compared to their counterparts to the northeast (C11-C17). The southwest canyons are located close to the shelf edge, where the upper continental slope is relatively steep and multiple landslides are imaged. We show that the thalwegs and walls of the southwest canyons were more actively eroded by sediment flows, with respect to the northeast canyons, making them deeper and steeper. Hence, submarine canyons in the southwest, with a more linear geometry, are now directly connected to the Pearl River Canyon. In parallel, seafloor fault scarps act as barriers for sediment transported to the heads of the northeast canyons. This research highlights how sediment supply, sediment pathways, and seafloor scarps can influence submarine canyon morphology along continental slopes. It contributes to a better understanding of the factors controlling canyon morphology worldwide.

Keywords: Seafloor morphology; Submarine canyons; Continental margin; Pearl River Mouth Basin; Northern South China Sea.

1. Introduction

Submarine canyons, comprising steep-walled valleys incised onto the continental shelf and slope, can form along all types of continental margin: divergent, convergent or transform (Mountjoy et al., 2009;

Harris and Whiteway, 2011; Puig et al., 2014). Submarine canyons have received considerable attention over the last few decades as they: (1) form major conduits for sediment and pollutants transported from shallow to deep marine environments (Mulder et al., 2012; Puig et al., 2013; Pope et al., 2019; Zhong et al., 2021), (2) are recognised as preferential locations for gas-hydrate and hydrocarbon accumulations (Mayall et al., 2006; Davies et al., 2012; Crutchley et al., 2017), and (3) record climatic change with a fine-enough resolution to allow palaeoceanographic reconstructions across continental margins (Zhu et al., 2010; Voigt et al., 2013).

Submarine canyons generally start evolving as submarine slides or slumps triggered by tectonic events, high sedimentation rates, rapid delta progradation, fluid seepage or fluid overpressure (Shepard, 1981; McHargue and Webb, 1986; Dugan and Flemings, 2000; Harris and Whiteway, 2011; Qin et al., 2017). Their development and morphology are influenced by a number of controlling factors, including sediment supply (Popescu et al., 2004; Puig et al., 2017), the eroding effect of downslope sediment flows (Orange, 1999; Puga-Bernabéu et al., 2013), tectonic activity (Popescu et al., 2004; Mulder et al., 2012), oceanographic currents (Mitchell, 2008; Puig et al., 2014) and even, in modern times, bottom trawling and anthropogenic structures (Martin et al., 2014). Such controlling factors greatly modify the morphology of submarine canyons at both their local and margin-wide scales (Goff, 2001; Jobe et al., 2011; Mulder et al., 2012). Therefore, understanding the factors that influence the morphology of submarine canyons can provide essential information on sediment transport processes and the modern sedimentary environment as a whole (Baztan et al., 2005; Puga-Bernabéu et al., 2013; Wiles et al., 2019; Naranjo-Vesga et al., 2022).

In recent years, an increasing number of researchers have studied the Shenhu Canyon System in the northern South China Sea, which comprises nineteen (19) closely spaced submarine canyons (Zhu et al., 2010; Gong et al., 2013; Ma et al., 2015; Zhou et al., 2015; Li et al., 2019; Yin et al., 2019; Su et al., 2020) (Fig. 1). This was due to the discovery of deep-water hydrocarbon prospects and extensive gas hydrate fields in the region (Zhu et al., 2009; Zhang et al., 2012). Previous work has addressed the sub-surface geological structures (He et al., 2014; Chen et al., 2016), internal architecture (Zhu et al., 2010; Gong et al., 2013; Ma et al., 2015; Zhou et al., 2015), and overall geological evolution (Gong et al., 2013; Ma et al., 2015; Zhou et al., 2015) of these submarine canyons, but scant research has focused on their seafloor geomorphology (e.g. Li et al., 2016; Yin et al., 2019). Significantly, the submarine canyons that form the Shenhu Canyon System reveal a differing morphology along the continental slope, with much steeper and more incised canyons occurring in the southwest when compared with their counterparts to the northeast (Fig. 2). Even so, there is still a lack of information about the factors controlling such morphological variations.

In this study, high-resolution bathymetric and two- and three-dimensional (2D/3D) seismic data are used to investigate the Shenhu Canyon System in the northern South China Sea (Fig. 1). The specific aims of this work are to: (a) quantitatively analyse the key geomorphologic features of the Shenhu Canyon System and related seafloor features; (b) investigate the main factors controlling the morphology of the Shenhu Canyon System; (c) discuss the effects of sediment supply, sediment transport pathways, and seafloor scarps on the morphology of closely spaced submarine canyons along a continental slope.

2. Geological setting

The South China Sea is a large semi-enclosed, marginal sea located at the junction between the Pacific, Indian-Australian and Eurasian tectonic plates (Taylor and Hayes, 1980). Sedimentary basins developing along its northern margin include, from west to east, the Yinggehai, Qiongdongnan, Pearl River Mouth and Taixinan basins (Fig. 1). The Pearl River Mouth Basin, where the Shenhu Canyon

System is located, is the largest sedimentary basin in the northern South China Sea (Fig. 1). Its evolution can be divided into two main stages (Yu, 1994): (1) early rifting and onset of tectonic subsidence from Late Cretaceous to the Middle Eocene; (2) regional thermal subsidence and tilting of the continental shelf, during which marine strata were accumulated from late Oligocene to the present day. In addition, three main tectonic events occurred in the Pearl River Mouth Basin during the Cenozoic: the Nanhai (ca. 32 Ma), Baiyun (ca. 23.8 Ma) and Dongsha (10.5 to 5.5 Ma) events (Dong et al., 2009; Pang et al., 2009; Wu et al., 2014). The Dongsha tectonic event affected the northeast part of the Pearl River Mouth Basin, having resulted in tectonic uplift, widespread faulting, magmatic activity and local erosion (Wu et al., 2014) (Fig. 1).

The Shenhu Canyon System is located at a water depth between 300 m and 1700 m, and records four distinct phases of evolution since 13.8 Ma (Ma et al., 2015). The heads of the submarine canyons are confined to the upper continental slope, south of a broad continental shelf with an average width of 236 km (Huang et al., 1995). Further south, the Shenhu Canyon System joins the E-W striking Pearl River Canyon, which forms one of the main conduits for sediment sourced from onshore areas into deep-water basins (Figs. 1 and 2a; Ding et al., 2013). The Pearl River Delta, to the northwest of the Shenhu Canyon System, has been a major source of sediment to the study area since the Late Oligocene (Fig. 1; Bao, 1995; Lüdmann et al., 2001; Lin et al., 2018).

3. Data and methods

Multibeam bathymetric and high-quality 2D/3D seismic data are used in this work (Figs. 1 and 2). The multibeam bathymetric data span an area of approximately 10,000 km^2, at a water depth of 200 m to 2600 m (Fig. 2a). The bathymetric data were acquired by the Guangzhou Marine Geological Survey, Ministry of Land and Resources, using a SeaBeam 2112 multibeam echosounder operating at a main frequency of 12 kHz with a pulse length of 3–20 ms. The raw multibeam bathymetric data were post-processed using CARIS HIPS and SIPS software, so to remove noise and correct for sound velocity variations within the water column. The resulting, processed bathymetric data were used to generate high-resolution seabed digital terrain models (DTM) with a grid resolution of 100 m. The DTMs were also used to generate slope-facing maps (aspect maps) and slope gradient maps using Global Mapper®.

The seismic data in this work were acquired and processed by the China National Offshore Oil Corporation (CNOOC) and interpreted on Kingdom© 2015 software. They were processed with a sampling interval of 4 ms and a bin spacing of 25 m × 12.5 m. The frequency bandwidth of the seismic data is 35-70 Hz, with a dominant frequency of 50 Hz, and their vertical resolution is ~10 m. The 2D seismic profiles have a frequency bandwidth of 30-45 Hz and were sampled at a rate of 4 ms, providing an average vertical resolution range between 15 m and 30 m. A water column velocity of 1530 m/s (Chen et al., 2016) was used to convert two-way travel time to true water depths in our analysis.

The quantitative analysis developed in this work follows the methods of Green et al. (2007), Covault et al. (2011), and Shumaker et al. (2018). A series of morphological profiles perpendicular to the thalwegs were extracted from the bathymetric datasets. The profiles were computed with a spacing of 50 m, decreasing to 25 m or less in areas of particular interest. In parallel, a series of longitudinal profiles along the canyon thalwegs and adjacent overbanks were extracted to highlight the morphological character of canyon incision. However, the data thus extracted are difficult to compare and contrast because of differences in canyon length and depth. To rectify this problem, we normalised the longitudinal profiles using the method in Covault et al. (2011). The canyons' geomorphological parameters measured in this work include total and straight canyon length, canyon sinuosity, depth of canyon incision, average canyon gradient along the canyon axis and relative to the north azimuth, the distance between canyon head and shelf edge, and the gradient of the slope between the canyon heads and shelf edge (Table 1).

4. Results

4.1. Shelf edge and slope morphology in the Pearl River Mouth Basin

4.1.1. Shelf edge

The shelf edge, or shelf break, is marked by an important change in slope gradient, and separates the flat-lying continental shelf from a steeper slope. The exact location of the shelf edge in clear on seismic profiles crossing the shelf and upper continental slope (Figs. 3 and 4b). The present-day shelf edge has a depth of ~300 m in the southwest part of the study area (Fig. 3a). To the northeast, however, the shelf edge occurs at a depth of ~200 m (Figs. 1 and 3). The bathymetric map of the study area shows that the shelf edge generally strikes to the NE, recording an abrupt change from SE to NE at a longitude of ~ 114.5°, near the southwest limit of the study area (Figs.1 and 2a).

Multiple shelf-edge deltas occur on the continental shelf (Figs. 3a and 4b). Seismic profiles crossing the southwest sector of the study area reveal a shelf edge to upper continental slope with southeast-prograding deltas, and associated clinoforms, dated as Pliocene to Quaternary in age (Ma et al., 2015; Zhou et al., 2021) (Figs. 3a and 4b). Series of mass-transport deposits (MTDs) are also observed close to these clinoforms (Fig. 4). The length and height of the slide scars of MTDs can be up to ~40 km and ~50 m, respectively (Figs. 2a and 4). In contrast, seismic profiles crossing the upper continental slope in the northeast sector of the study area reveal Pliocene-Quaternary strata as being continuous, parallel or subparallel in character (Figs. 3c and 5b).

4.1.2. Slope morphology

Seismic profiles covering the continental shelf and slope of the Pearl River Mouth Basin reveal two different types of continental slope (Fig. 3). Due to the presence of the Pearl River Canyon and Baiyun Slide Complex downslope, seismic lines crossing the southwest part of the study area show a concave slope (Figs. 3a and 3b). The continental slope is relatively steep in its upper part, where a maximum gradient of ~2.5° is reached, becoming gentler towards its base (Figs. 3a and 3b). In contrast, the seismic profiles crossing the northeast part of the study area reveal a convex slope with a relatively gentle (~0.3°) upper slope and a steep (~2°) lower slope (Fig. 3c).

4.2. Pearl River Canyon and linear depressions

The Pearl River Canyon is sinuous in plan view and divided into three distinct reaches with differing orientations (Figs. 1 and 2a). The upper reach lies on the shelf edge and upper continental slope, striking to the SE (Fig. 2a). Several small-scale channels, with their heads incising the shelf edge, show a V-shaped section on the upper reach, with a maximum incision depth of ~70 m and a width of ~2 km (Fig. 2a). In comparison, the middle reach of the Pearl River Canyon extends for a distance of ~80 km, changing to a predominant E-W strike at a water depth of ~1200 m (Fig. 2a). Lower on the continental slope, at a water depth of ~2100 m, the general strike of the middle reach changes from nearly E-W to NW-SE until one finds the continental rise (Figs. 1 and 2a). Seamounts are located near the boundary between the middle and lower reaches of the Pearl River Canyon (Fig. 2a). It should be noted that a giant submarine slide, the Baiyun Slide Complex, is also observed in this area as shown by its prominent seabed scarp (Fig. 2a). It is the largest submarine landslide near the Pearl River canyon (Fig. 2a). The Baiyun Slide Complex spans an area of ~ 11000 km^2, comprising multi-stage overlapping submarine landslide deposits (Fig. 2a). The headwall of the Baiyun Slide Complex displays an arcuate scarp, with a length of ~250 km and an average height of up to ~130 m (Figs. 2a, 2e and 3a).

Aspect maps can help to identify seafloor features with spurious strikes, highlighting the presence of seafloor depressions, sidewalls, gullies and local variations in slope gradient (McAdoo, 2000). Continuous and linear depressions are identified in the lower reaches of the Shenhu Canyon System and Pearl River Canyon on the seafloor aspect map (Fig. 6). Their length varies from a few kilometers to tens of kilometers, with a depth ranging from a few meters to tens of meters (Fig. 6). It should be stressed that a series of linear depressions were developed on the canyon head in the southwest part of the study area (e.g. C3-C7, C9), and some these depressions can be traced from the canyon heads up to the shelf edge (e.g. C3, C4, C7) (Fig. 6b). They are up to ~1 km wide and ~100 m deep (Fig. 6d). However, linear depressions in the canyons to the northeast do not extend to the shelf edge. Those that extend downslope from the canyon mouths are shown to bypass the seamounts, to finally enter the lower reach of Pearl River Canyon (Fig. 6).

4.3. Shenhu Canyon System

4.3.1 General geomorphology

The Shenhu Canyon System consists of 19 submarine canyons, herein named C1 to C19, following a southwest to northeast direction (Fig. 2a). They do not erode the shelf edge and are thus classified as slope-confined canyons, with their heads located at a water depth between 350 m to 880 m (Table 1). Submarine canyons are 13 km to 36 km long, displaying V-shaped cross-sections in their upper reaches and U-shaped cross-sections in their lower reaches (Fig. 2). The bathymetric data show they are wider downslope, ranging from 2 km to 5 km in width. All these submarine canyons have no obvious branches at their heads and exhibit a relatively straight thalweg with an NW-SE orientation, except for C17 and C18 (Fig. 2a and Table 1). Importantly, canyons C3 to C10 can be traced into the middle reach of the Pearl River Canyon, whereas the lower reaches of canyons C5 to C10 have been eroded by the Baiyun Slide Complex (Fig. 2a and 2e). In the northeast part of the study area, canyons C11 to C17 terminate 8 km to 50 km before reaching the Baiyun Slide Complex, though smaller-scale linear depressions on their downslope prolongation still enter the lower reach of the Pearl River Canyon (Figs. 2a and 6).

4.3.2. Morphological analysis of submarine canyons

Canyons C18 and C19 in the northeast portion of Shenhu Canyon System are not fully imaged by our bathymetric data (Fig. 2a). A detailed analysis of canyons C1 to C17 reveals gradual variations in morphological parameters such as the water depth of canyon heads, the depth of canyon incision, the average slope gradient along the canyon thalweg, and the slope gradient of the canyon walls (Table 1).

The canyon heads of C1 to C17 do not incise the shelf, lying on the upper continental slope at a water depth from 350 m to 730 m (except for C8) (Table 1). In addition, the depth of the canyon heads increases markedly from southwest to northeast (Fig. 7a). The canyon heads of C1 to C10 occur at water depths between 350 m and 580 m (except for C8), while the heads of C11-C17 are observed at a water depth ranging from 660 m to 730 m (Figs. 2a and 7a). Longitudinal profiles along the canyon thalwegs shows that canyons in the southwest (e.g. C3-C7, C9-C11) have concave-upward profiles, while canyons to the northeast (e.g.C12-C16) have slightly concave profiles (Fig. 8). Their maximum incision depth varies from 150 m to 412 m, decreasing from southwest to northeast, except for C1 and C2 (Fig. 7b and Table 1). The maximum incision depth of canyons C3-C10 varies from 288 m to

412 m in the southwest part of the study area, while it varies from 155 m to 270 m for C11-C17, in the northeast (Fig. 7b). The average slope gradient along the canyon thalwegs ranges from ~1.5° to ~2.3° (Table 1) and shows a decreasing trend from southwest to northeast (Fig. 7c). Canyons C1-C10 in the southwest have relatively steeper canyon walls, with their maximum slope gradient reaching ~20° (Fig. 9a). Canyons to the northeast (C11-C17) have wall gradients of less than ~15° (Fig. 9a). The distance between canyon heads and the shelf edge varies from 1.6 km to 61 km, revealing an increasing trend from southwest to northeast (Fig. 10a and Table 1). In the southwest, the distance between the canyon heads and shelf edge varies from 1.6 km to 8 km (except for canyon C8) and the slope gradient ranges from ~1.8° to ~2.7° (Figs. 9a and 10). However, the canyons to the northeast reveal a longer distance (20-61 km) between their heads and the shelf edge (Fig. 10a). The seafloor in the upper part of their heads is relatively flat, with an average slope gradient ranging from ~0.4° to ~1.1° (Figs. 9a and 10b).

As described, the submarine canyons in the Shenhu Canyon System show morphological variations that follow a southwest-northeast trend along the continental slope. The incision depth, average slope gradient along the canyon thalwegs, the slope gradient of the canyon walls, and the gradient of the seafloor between canyon heads and shelf edge, all decrease towards the northeast. Conversely, the water depth of canyon heads, and the distance between canyon heads and the shelf edge, increase towards the northeast.

4.3.3. Evolution stages of the Shenhu Canyon System

The development of the Shenhu Canyon System has been divided into multi-evolutionary phases based on its internal seismic facies. Seismic profiles crossing the study area reveal that small individual canyons were initially formed in the Middle Miocene at ~13.8 Ma (Fig. 11). The size of the interpreted canyons is greater, and their spacing relatively smaller, from 12.5 Ma to 10.5 Ma (Fig. 11). Seismic reflections show poor continuity and the presence of multiple MTDs after 10.5 Ma in the northeast part of the Shenhu Canyon System, likely because the Dongsha tectonic event resulted in significant basement uplift (Figs. 1 and 11). A series of small canyons were then developed in the northeast part of the Shenhu Canyon System and incised upper Miocene strata data from 10.5 Ma onwards (Fig. 11). However, they were completely filled and buried by younger strata, comprising continuous, parallel or subparallel seismic reflections, after 5.5 Ma (Fig. 11).

4.4 Faults and related seafloor scarps

A basement high is identified on a seismic profile crossing canyons C3 to C19, with its depth below the seafloor increasing to the southwest (Fig. 11). Several normal faults associated with this basement high are identified on the upper continental slope (Fig. 5). Some of the faults dipping opposite to the slope gradient reach the seafloor to form prominent seafloor scarps with heights of tens of meters or more (Figs. 5a and 9). The high-quality bathymetry data interpreted in this work also reveals a series of seafloor scarps, with lengths of 5-15 km in the northeast part of the study area (Figs. 2a and 9). Faults mainly strike E-W to WNW-ESE, perpendicularly to the strike of present-day canyons (Figs. 2a and 9a).

5. Discussion

The geomorphological data in this work stress the important differences observed between the northeast and southwest portions of the Shenhu Canyon System in terms of their incision depth, slope gradient of canyon thalwegs and slope gradient of their walls (Figs. 2b, 7b, 7c and 9a). Canyons in the southwest have greater incision depths, steeper canyon thalwegs, and steeper canyon walls (Figs.

7b, 7c and 9a). In the following sections, the factors controlling the morphology of the Shenhu Canyon System are discussed.

5.1. Canyon morphology as a function of sediment supply

Shelf-edge deltas play a critical role in the partitioning and delivery of sediment to the continental slope and basin floor (Gong et al., 2019; Liu et al., 2019). A deltaic succession developed on the shelf edge from the Pliocene to the Quaternary in the northwest part of the study area (e.g. Bao, 1995; Lüdmann et al., 2001; Lin et al., 2018; Liu et al., 2019; Wang et al., 2020) (Figs. 1, 3a and 4b). All prodelta fronts reveal important progradation and, consequently, deltas have prograded onto the outer shelf (Figs. 3a and 4b). Previous studies demonstrated that the Pearl River deltas have prograded 10-15 km for the past 478 ky in the form of a broad sediment apron over the pre-existing shelf edge (Gong et al., 2019), due to high sediment supply (Liu et al., 2019; Su et al., 2019; Wang et al., 2020). Shelf-edge deltas spilling over the shelf edge can guarantee the delivery of terrestrial sediment to deep-water basins regardless of relative sea-level position (Covault and Graham, 2010; Gong et al., 2019).

In the southwest part of the study area, sediment transported by deltaic systems onto the shelf margin resulted in a series of progradational, sigmoidal clinoforms (Figs. 2a, 4 and 9a). As a result of this setting, the average seafloor gradient increases from ~0.1° on the shelf to ~2.5° on the upper continental slope (Figs. 3a, 3b and 9a). The high sediment supply and relatively steep upper continental slope promote seafloor instability and, accordingly, a series of slide scars are observed in bathymetric data close to the canyon heads in the southwest (Figs. 2a, 4a and 9a). Similarly, multiple MTDs are identified in between Pliocene-Quaternary clinoforms near the canyon heads (Fig. 4b). Mass-wasting events originating from the shelf edge likely account for a significant portion of sediment supplied to the canyons in the southwest part of the study area. In this same region, information gathered from gravity and piston cores suggest a large amount of shelf-derived, coarse sediment on the upper continental slope (Wang et al., 2018; Gong et al., 2019), indicating that gravity flows are active (and abundant) in this region. This is consistent with the fact that longitudinal profiles along the canyon thalwegs in the southwest reveal a concave-upward morphology, while canyons to the northeast show a slight concave-upward geometry (Fig. 8). Such a difference is due to the fact that southwest canyons have suffered relatively stronger erosion (e.g. Mitchell, 2005; Covault et al., 2011). In contrast, seismic profiles crossing the upper continental slope in the northeast reveal continuous, parallel or subparallel Pliocene-Quaternary strata (Figs. 3c and 5b). This shows that the northeast sector of the study area is not frequently affected by mass movements (He et al., 2014; Ma et al., 2015).

Downslope-eroding gravity flows derived from the shelf and upper continental slope, or generated by downslope flow transformation of canyon-walls landslides, are common mechanisms promoting axial incision in submarine canyons (Parsons et al., 2007; Rebesco et al., 2009; Puga-Bernabéu et al., 2013). The walls of canyons C1-C10 in the southwest are steeper (up to ~20°) than those of canyons C11-C17 in the northeast (less than ~15°) (Fig. 9a). Steeper canyon walls undoubtedly result in a higher probability of slope instability. This is consistent with the results in Chen et al. (2016) proving that the number of landslides and slumps on canyon walls decreases from southwest to northeast in the study area. Downslope-eroding gravity flows generated by the unstable canyon walls are considered to promote axial canyon incision (Parsons et al., 2007; Puga-Bernabéu et al., 2013). Therefore, canyons in the southwest were likely eroded more frequently by gravity flows than those in the northeast, promoting their greater depth and the formation of steeper thalwegs.

5.2. Influence of sediment pathways on canyon morphology

The dimension of submarine canyons is closely controlled by slope morphology (Naranjo-Vesga et al., 2022). The orientation of the sediment flow pathways is controlled by the slope gradient, as these flows will tend to be directed towards topographic lows (Kneller et al., 2016; Naranjo-Vesga et al., 2022). The Pearl River Canyon and Shenhu Canyon System constitute the main topographic lows for sediment transported from shallow to deep waters in the Pearl River Mouth Basin (Fig. 2; Ding et al., 2013). Previous studies have shown that the Pearl River Canyon began its development at ~21 Ma (Ding et al., 2013; Chen et al., 2020), i.e. much earlier than the Shenhu Canyon System, which started to form at ~13.8 Ma (Fig. 11). After the Shenhu Canyon System was formed, it gradually became the main sediment conduit on the continental slope by replacing the upper reach of the Pearl River Canyon (Ding et al., 2013; Su et al., 2020). Later, the lower reaches of canyons C5 to C10 were eroded by the Baiyun Slide Complex, creating prominent seafloor scarps oriented perpendicularly to these canyons (Figs. 2a, 2e, 3a and 6; Li et al., 2014). The seafloor depression, or relative low, generated by the Pearl River Canyon and Baiyun Slide Complex provided abundant accommodation space for sediment derived from submarine canyons in the Shenhu Canyon System (Figs. 2a, 2e, 3a and 6). Due to the presence of the Pearl River Canyon and Baiyun Slide Complex downslope, the continental slope shows a concave-upward morphology that can be associated with the high sediment supply recorded in the southwest part of the study area (Adams et al., 1998; Patruno et al., 2015; Zhuo et al., 2019). Similarly, concave-upward slopes have been observed in other parts on the northern South China Sea margin, such as in the Yinggehai and western Qiongdongnan basins (Zhuo et al., 2019). These basins are characterised by their rapid sediment progradation, suggesting they are preferential areas for sediment transport.

We note that the lower reaches of the southwest canyons C3-C10 are directly connected to the middle reach of the Pearl River Canyon. Conversely, a series of seamounts is present between the lower reaches of the northeast canyons C11-C17 and the Pearl River Canyon (Figs. 2a and 6). In addition, canyons C1-C10 in the southwest are closer to the shelf edge when compared to canyons C11-C17 to the northeast (Figs. 1, 2a and 10a). The distance between canyon heads and the shelf edge increases significantly from southwest (~1.6 km) to northeast (61 km) (Figs. 2a, 10a and Table 1), whereas the average seafloor gradient between canyon heads and the shelf edge decreases from ~2.5° to ~0.4° towards the northeast (Figs. 9a and 10b). As sediment flows inevitably move downslope in the direction of maximum dip, they are highly sensitive to seafloor topography and gradient (Kneller et al., 2016; Naranjo-Vesga et al., 2022). This suggests that sediment flows along the shelf edge and upper continental slope were more easily funneled into the canyon heads in the southwest part of the study area.

The aspect map of the study area reveals the presence of linear depressions that are an order of magnitude smaller than the submarine canyons. The linear depressions extend from the downslope termination of the canyons in the Shenhu Canyon System to the middle reach of the Pearl River Canyon (Fig. 6). It should be noted that some linear depressions can be traced from canyon heads to the shelf edge in the southwest part of the study area (e.g. canyons C3, C4 and C7). Previous work suggested that such linear depressions within canyons are troughs eroded by high-frequency sediment flows (Field et al., 1999; Orange, 1999; Kneller et al., 2016; Shumaker et al., 2017; Wang et al., 2017; Li et al., 2020). Once developed, such troughs are able to control the paths of sediment flows by funnelling them (Normandeau et al., 2022). The distribution of linear depressions in the study area illustrates that canyons in the southwest, with more linear depressions in their upslope and downslope regions (Fig. 6), would have been more eroded by gravity flows. This indicates that the southwest canyons, when compared with the canyons in the northeast, formed preferential pathways for sediment transported from shallow to deep waters. We infer that in the area of the Shenhu Canyon System, high-frequency sediment gravity flows along the depressions were sourced from larger-scale canyons in the part of the slope with the highest gradient. The fact that these depressions can only be traced from the canyon heads to the shelf edge in the southwest part of the study area (Fig. 6), and that the southwest canyons are much deeper and steeper than those in the northeast (Figs. 7b and 7c), confirms that sediment gravity flows are more active in the southwest part of the Shenhu Canyon System. This also means this part of the canyon system effectively replaced the upper reaches of the Pearl River Canyon in transferring sediment from shallow to deep waters (Fig. 12). This made the southwest canyons much deeper and steeper than those in the northeast.

5.3. Effect of seafloor scarps on canyon morphology

Previous studies proposed tectonic uplift as a major influence on submarine canyon morphology (Mountjoy et al., 2009; Harris and Whiteway, 2011; Mulder et al., 2012; Tournadour et al., 2017). The most prominent example is that of submarine canyons on the northern slope of the Little Bahama Bank (Mulder et al., 2012). In this region, the geometry of submarine canyons varies along a west-east trending bank slope. The eastern canyons in the Little Bahama Bank are longer, deeper, wider and more incised than those in the west of the bank (Mulder et al., 2012; Tournadour et al., 2017). Differences in canyon morphology were considered to result from tectonic tilting of the entire carbonate margin to the west during the Cenozoic (Mulder et al., 2012).

A series of tectonic events have occurred in and around our study area during the Cenozoic, i.e. the Nanhai (ca. 32 Ma), Baiyun (ca. 23.8 Ma) and Dongsha (ca. 10.5 to 5.5 Ma) events (Dong et al., 2009; Pang et al., 2009; Wu et al., 2014). Submarine canyon development in the Shenhu Canyon System was largely affected by the Dongsha tectonic event (Fig. 1; Ma et al., 2015; Zhou et al., 2015), which caused significant uplift in its northeast part (Figs. 3c, 5a and 11). At the time of the Dongsha tectonic event, still in the northeast part of the study area, seismic reflections show poor continuity and the presence of multiple MTDs (Fig. 11). This suggests the occurrence of frequent sediment flows and an unstable sedimentary environment in this area. A series of smaller canyons are observed in upper Miocene strata in the northeast part of the Shenhu Canyon System (Fig. 11). However, these small canyons disappear in the northeast, and are replaced by continuous, parallel or subparallel seismic reflections after 5.5 Ma (Fig. 11). This fact indicates that quieter open-slope conditions replaced the previous sediment flows and erosion may have already ceased after 5.5 Ma in this region. In addition, the present-day submarine canyons in the northeast part of the Shenhu Canyon System are smaller and less incised compared to those in the southwest (Figs. 2b and 7b), and a series of seafloor scarps can be observed above the canyon heads in the northeast of our study area (Figs. 3c, 5a and 9). We postulate that tectonic uplift resulting from the Dongsha tectonic event does not significantly influence submarine-canyon morphology at present, even though it may have played a vital role in the past and may have generated the still-present rugged seafloor in the northeast of our study area (Figs. 3c, 5a and 9).

Canyon morphology can also be affected by a rugged seafloor topography above the canyon heads (Puga-Bernabéu et al., 2013). Puga-Bernabéu et al. (2013) have shown that the morphology of submarine canyons varies along the Great Barrier Reef margin offshore northeastern Australia. Submarine canyons with extensive barrier reefs in their upper regions are less incised and, thus, were interpreted as slope-confined canyons. Conversely, submarine canyons with no well-defined barrier reefs are deeply incised on the continental shelf, and sediment supply to these canyons is larger compared to slope-confined canyons. Thus, the presence of barrier reefs at the shelf edge is considered as one of the main factors controlling canyon morphology in the Ribbon Reef region

(Puga-Bernabéu et al., 2013).

In the study area, a series of normal faults related to local tectonic uplift are observed close to the heads of canyons C16-C19 (Figs. 3c and 5). They offset the modern seafloor, resulting in the formation of scarps that are up to 60 m tall (Figs. 3c, 5a and 9). These scarps are WNW-SEE striking and act as physical barriers for sediment flows derived from the shelf edge (Figs. 5a, 9 and 12). The root-mean-square (RMS) amplitude maps published in Ma et al., (2015) reveal obvious differences on both sides of the scarps. High RMS amplitudes are located on the north side of the scarps, while their southern sides show low RMS amplitudes. This implies that a large volume of coarse-grained sediment is deposited on the north side of the scarps (Ma et al., 2015). The lack of seafloor scarps close to the heads of canyons C1 to C15 suggests the absence of bathymetric obstacles and greater sediment transport across the continental shelf and upper continental slope than those reported in Ma et al. (2015) (Fig. 12). If existent, seafloor scarps would have formed physical barriers for sediment transported to the canyon heads, making the northeast canyons less eroded by sediment flows.

The data in this work thus show that the canyons in the southwest part of the Shenhu Canyon System are more incised by sediment flows than those in its northeast part, as they are closer to the Pearl River delta and lack any bathymetric traps (faults scarps) for incoming sediment.

6. Conclusions

The Shenhu Canyon System of the northern South China Sea constitutes a unique case study that to improve our understanding on the factors controlling the morphology of closely spaced submarine canyons. A combination of high-resolution bathymetric, 2D/3D seismic data were therefore used in this study to investigate morphological variations in the Shenhu Canyon System of the northern South China Sea. The main conclusions of this work are as follows:

(1) The Shenhu Canyon System consists of nineteen (19) submarine canyons showing a variable morphology along the continental slope, from southwest to northeast. Canyons in the southwest have greater incision depths, steeper canyon walls, and steeper thalwegs than those in the northeast.

(2) The differing canyon morphology observed in the study area suggests the effect of multiple controlling factors, both regional and local, throughout the evolution of the Shenhu Canyon System. Sediment supply, preferential pathways for sediment, and the presence of seafloor scarps, are main factors controlling the morphology of the studied submarine canyons.

(3) Canyons C1 to C10 are close to the shelf edge, where numerous landslides occurred in the past. They are connected to the Pearl River Canyon and reveal an open upper continental slope with no seafloor scarps. They act as preferential pathways for sediment transported from the shelf edge into the Pearl River Canyon. The canyon walls of canyons C1-C10 to the southwest are also steeper (up to ~20°), resulting in a higher instability of its walls. These conditions allow for higher sediment supply and frequency of sediment flows, intensifying canyon erosion.

(4) In the northeast of the study area, the upper continental slope is characterised by a broad, low gradient seafloor, probably associated with fewer sediment flows. The northeast canyons C11-C17 developed far from the shelf edge and have relatively gentle canyon walls (<15°). This makes them less likely to be eroded by sediment flows sourced from the shelf edge, upper continental slope, and canyon walls. In addition, seafloor scarps on the seafloor have limited the transport of sediment to the Shenhu Canyon System. Consequently, the northeast canyons were less eroded by sediment flows.

Acknowledgments

We acknowledge China National Offshore Oil Corporation for their permission to release the seismic data. This work was financially supported by Guangdong Basic and Applied Basic Research Foundation (No.

2020B1515020016), National Natural Science Foundation of China (No. 42206069), National Natural Science Foundation of China (No. 41876054), Key Laboratory of Ocean and Marginal Sea Geology, Chinese Academy of Sciences (No. OMG2020-09), and Guangzhou Basic and Applied Basic Research Program (No. 202201010488). Dr. Wei Li is specially funded by the CAS Pioneer Hundred Talents Program (Y8SL011001). We appreciate the Editor Prof. Zhongyuan Chen and three anonymous reviewers for their constructive comments, which greatly help us to improve the quality of our manuscript.

Figure and table captions

Figure 1: Combined topographic and bathymetric maps of the northern South China Sea margin. The orange dashed lines highlight the boundaries of four major deep-water sedimentary basins in the northern half of the South China Sea. The location of the present shelf edge is indicated by the black dashed line (modified from Huang et al. (2021) and Zhuo et al. (2019)). The Shenhu Canyon System shown in the red box is connected with the ancient Pearl River delta (marked by the shadow in blue) in the upper slope region and the Pearl River Canyon (indicated by the purple dotted line) in the downslope area. The distribution of the ancient Pearl River delta is based on Bao (1995) and Lüdmann et al. (2001). The area affected by Dongsha Tectonic Event is shown by the orange shadowing (Wu et al., 2014).

Figure 2: (a) Bathymetry map derived from multibeam bathymetric and 3D seismic data revealing the detailed seafloor morphology of Shenhu Canyon System and Pearl River Canyon. The polygons with grey dotted lines represent the coverage of multibeam bathymetric data. The main sediment fairway of the Pearl River Canyon is shown by a purple dashed line. The blue dashed arrows indicate the locations of several submarine small-scale channels in the upper reaches of Pearl River Canyon.

Seafloor scarps in the northeast part of the study area are marked by black dotted lines. (b) Bathymetric profile across canyons C1 to C17 showing canyon incision to decrease from southwest to northeast, except for C1 and C2. (c) Bathymetric profile across the upper reach of canyons C3 to C4 displaying V-shaped morphologies. (d) Bathymetric profile across the lower reach of canyons C3 to C4 displaying U-shaped morphologies. Note that Fig. 2c and Fig. 2d have the same horizontal and vertical scales. The red lines indicate the variations of slope gradients along the bathymetric profiles in Fig. 2b, 2c and 2d. (e) Three-dimensional view of the Baiyun Slide scarps highlighting the lower reaches of canyons C5 to C10 as having been eroded by the Baiyun Slide.

Figure 3: (a) Two-dimensional (2D) seismic profile crossing the westernmost part of study area showing the steeper upper continental slope (~2.5°) and the presence of prograding shelf-edge delta and clinoform seismic facies, the shelf edge, the Baiyun Slide scarps, and the Pearl River Canyon. (b) NW-SE oriented two-dimensional (2D) seismic profile depicting the slope geometry in the southwest part of the Pearl River Mouth Basin. Here, the slope is generally concave and the upper continental slope is steeper (~2.5°) to the lower slope (~0.7°). (c) Two-dimensional (2D) seismic profile with a NW-SE orientation imaging the continental slope in the northeast part of the Pearl River Mouth Basin. Here, the slope is convex with a gentle upper slope (~0.3°) and a relatively steep lower slope (~2°). Note that several faults offset the seafloor to form prominent scarps. Locations of profiles are shown in Fig. 1.

Figure 4: (a) Bathymetric map highlighting the detailed seafloor morphology of the shelf edge in the west of study area. Note that a series of slide scars developed near the shelf edge. See Fig. 2a for location. (b) Two-dimensional (2D) seismic profile crossing the upper continental slope and C9

showing the major depositional features, including a shelf-edge delta with clinoforms, MTDs, and small submarine channels at the shelf edge to the upper continental slope. The stratigraphic interpretation in this figure follows the framework of Ma et al. (2015) and Zhou et al. (2021). See Fig. 2a for the location of the seismic profile.

Figure 5: (a) Seismic profile from three-dimensional (3D) seismic data crossing the northeast part of the Shenhu Canyon System revealing the presence of a large scarp, ~60 m high, generated when of the uplift of the basement high to the NE. Faults are marked by red solid lines. See Fig. 2a for the location of the seismic profile. (b) Two-dimensional (2D) seismic profile crossing the upper continental slope and C16. Several faults can be observed on the upper continental slope, as marked by red solid lines. Note the seismic facies replaced by continuous, parallel or subparallel seismic reflections after 5.5 Ma on the upper continental slope. The stratigraphic interpretation in this figure follows the framework of Ma et al. (2015).

Figure 6: (a) Slope-facing map (aspect map) of the study area derived from multibeam data. The map represents the direction of slope gradient. The aspect map is important to highlight the downslope trending continuous linear depressions. (b) Line-drawn interpretation of Fig. 6a revealing the wide linear depressions in the study area, features that suggest significant erosion by sediment flows. The white dotted arrows indicate the location of linear depressions and sediment transport pathways. (c) Bathymetric profile across the continental slope revealing the presence of multiple seafloor depressions. They can be up to tens of meters in depth. (d) Bathymetric profile across the upper continental slope between the canyon heads and the shelf edge revealing the presence of multiple seafloor depressions.

Figure 7: Variations in the morphological parameters of submarine canyons. The red dotted lines highlight the variations in trend of morphological parameters. (a) The depth of canyon heads shows an increasing trend from southwest to northeast, except for C8. (b) The maximum canyon incision shows a decreasing trend from southwest to northeast, except for C1 and C2. (c) The average canyon gradient along the axial thalwegs of submarine canyons shows a decreasing trend from southwest to northeast.

Figure 8: (a) Longitudinal profiles along the canyon thalwegs of submarine canyons C1-C17. (b) Normalized plots of the longitudinal profiles along the canyon thalwegs and adjacent overbanks highlighting the character of canyon incision in the study area. It should be noted that canyons C4 and C7 in the southwest have concave-upward profiles along their thalwegs, while canyons to the northeast (C12 and C15) have slightly concave profiles.

Figure 9: (a) Slope gradient map of the Shenhu Canyon System highlighting the fact that the walls of canyons in the southwest (C1-C10) are steeper than those in the northeast (C11-C17). The black dotted lines indicate the locations of seafloor scarps in the northeast part of the study area. (b) Three-dimensional view of the slope gradient of the upper slope in the northeast part of Shenhu Canyon System. Note that a series of seafloor scarps developed on the upper continental slope. (c) Bathymetric profile crossing the upper continental slope revealing the presence of seafloor scarps. See Fig. 9b for the location of the bathymetric profiles.

Figure 10: Variations in morphological parameters of the upper continental slope. The red dotted lines

highlight the variation trend of morphological parameters. (a) Distance between the canyon heads and shelf edge displaying an increasing trend from southwest (~1.6 km) to northeast (~61 km). (b) The average seafloor gradient between shelf edge and canyon heads shows a decreasing trend from southwest (~2.1°) to northeast (~0.3°).

Figure 11: (a) Seismic profile gathered from 3D seismic data revealing the detailed internal architecture of submarine canyons C3 to C19. Location of the seismic profile in Fig. 2a. The development of the submarine canyons can be divided into four stages according to Ma et. al (2015). Note that the significant tectonic uplift in the northeast part of the Shenhu Canyon System. (b) Zoomed-in seismic section in Fig. 11a showing that the scales of submarine canyons decrease to the northeast. Note that few submarine canyons can be identified in the northeast part of the Shenhu Canyon System, especially above the basement high uplifted after the end of Late Miocene (5.5 Ma).

Figure 12: Three-dimensional view of a conceptual model highlighting the main sedimentary processes occurring in the study area. In the southwest part of the study area, canyons are close to the shelf edge where numerous landslides and sediment flows have developed. They connect with the Pearl River Canyon and show an open upper continental slope lacking seafloor scarps, which act as the preferential pathways for sediment transported from the shelf edge into the Pearl River Canyon. In the northeast part of the study area, the upper continental slope is characterized by a broad, low-gradient seafloor, with fewer sediment flows. The fault scarps act as physical barriers on the seafloor, limiting the transport of sediment to the northeast canyons.

Table 1: Summary of the main characteristics of submarine canyons in the Shenhu Canyon System

C: canyons; HD: depth at canyon head; TD: depth at canyon end; L: total length (distance between canyon head and canyon mouth measured along the canyon thalweg); SL: straight length (shortest distance between canyon head and canyon mouth); S: sinuosity (ratio between the total and straight length); MI: difference in maximum canyon incision depth between the canyon axis and the adjacent overbanks; CGr: average canyon gradient along the canyon axes relative to horizontal; Az: azimuth (orientation relative to north between the starting and ending points); D: distance between canyon head and shelf edge; SGr: slope gradient of the continental slope between the canyon heads and the shelf edge.

References

Adams, E.W., Schlager, W., Wattel, E., 1998. Submarine slopes with an exponential curvature. Sedimentary Geology 117, 135-141. https://doi.org/10.1016/S0037-0738(98)00044-X.

Bao, C., 1995. Buried ancient channels and deltas in the Zhujiang River mouth shelf area. Marine Geology & Quaternary Geology 15, 25-34 (in Chinese with English abstract). doi: 10.16562/j.cnki.0256-492.1995.02.004.

Baztan, J., Berné, S., Olivet, J.L., Rabineau, M., Aslanian, D., Gaudin, M., Réhault, J.P., Canals, M., 2005. Axial incision: The key to understand submarine canyon evolution (in the western Gulf of Lion). Marine and Petroleum Geology 22, 805-826. https://doi.org/10.1016/j.marpetgeo.2005.03.011.

Covault, J.A., Graham, S.A., 2010. Submarine fans at all sea-level stands: Tectono-morphologic and climatic controls on terrigenous sediment delivery to the deep sea. Geology 38, 939-942. https://doi.org/10.1130/g31081.1.

Covault, J.A., Fildani, A., Romans, B.W., McHargue, T., 2011. The natural range of submarine canyon-and-channel longitudinal profiles. Geosphere 7, 313-332. https://doi.org/10.1130/ges00610.1.

Chen, D.X., Wang, X.J., Völker, D., Wu, S.G., Wang, L., Li, W., Li, Q.P., Zhu, Z.Y., Li, C.L., Qin, Z.L., Sun, Q.L., 2016. Three dimensional seismic studies of deep-water hazard-related features on the northern slope of South China

Sea. Marine and Petroleum Geology 77, 1125-1139. https://doi.org/10.1016/j.marpetgeo.2016.08.012.

Chen, H., Xie, X., Mao, K., He, Y., Su, M., Zhang, W., 2020. Depositional Characteristics and Formation Mechanisms of Deep-Water Canyon Systems along the Northern South China Sea Margin. Journal of Earth Science 31, 808-819. https://doi.org/10.1007/s12583-020-1284-z.

Chen, H., Xie, X., Zhang, W., Shu, Y., Wang, D., Vandorpe, T., Van Rooij, D., 2016. Deep-water sedimentary systems and their relationship with bottom currents at the intersection of Xisha Trough and Northwest Sub-Basin, South China Sea. Marine Geology 378, 101-113. https://doi.org/10.1016/j.margeo.2015.11.002.

Crutchley, G.J., Kroeger, K.F., Pecher, I.A., Mountjoy, J.J., Gorman, A.R., 2017. Gas Hydrate Formation Amid Submarine Canyon Incision: Investigations From New Zealand's Hikurangi Subduction Margin. Geochemistry, Geophysics, Geosystems 18, 4299-4316. https://doi.org/10.1002/2017gc007021.

Davies, R.J., Thatcher, K.E., Mathias, S.A., Yang, J., 2012. Deepwater canyons: An escape route for methane sealed by methane hydrate. Earth and Planetary Science Letters 323-324, 72-78. https://doi.org/10.1016/j.epsl.2011.11.007.

Ding, W., Li, J., Li, J., Fang, Y., Tang, Y., 2013. Morphotectonics and evolutionary controls on the Pearl River Canyon system, South China Sea. Marine Geophysical Research 34, 221-238. https://doi.org/10.1007/s11001-013-9173-9.

Dong, D.D., Zhang, G.C., Zhong, K., Yuan, S.Q., Wu, S.G., 2009. Tectonic Evolution and Dynamics of Deepwater Area of Pearl River Mouth Basin, Northern South China Sea. Journal of Earth Science 20, 147-159. https://doi.org/10.1007/s12583-009-0016-1.

Dugan, B., Flemings, P.B., 2000. Overpressure and fluid flow in the New Jersey continental slope: Implications for slope failure and cold seeps. Science 289, 288-291. https://doi.org/10.1126/science.289.5477.288.

Field, M.E., Gardner, J.V., Prior, D.B., 1999. Geometry and significance of stacked gullies on the northern California slope. Marine Geology 154, 271-286. https://doi.org/10.1016/s0025-3227(98)00118-2.

Goff, J.A., 2001. Quantitative classification of canyon systems on continental slopes and a possible relationship to slope curvature. Geophysical Research Letters 28, 4359-4362. https://doi.org/10.1029/2001gl013300.

Gong, C., Steel, R.J., Wang, Y., Sweet, M.L., Xian, B., Xu, Q., Zhang, B., 2019. Shelf-edge delta overreach at the shelf break can guarantee the delivery of terrestrial sediments to deep water at all sea-level stands. Aapg Bulletin 103, 65-90. https://doi.org/10.1306/05111816171117230.

Gong, C.L., Wang, Y.M., Zhu, W.L., Li, W.G., Xu, Q., 2013. Upper Miocene to Quaternary unidirectionally migrating deep-water channels in the Pearl River Mouth Basin, northern South China Sea. Aapg Bulletin 97, 285-308. https://doi.org/10.1306/07121211159.

Green, A.N., Goff, J.A., Uken, R., 2007. Geomorphological evidence for upslope canyon-forming processes on the northern KwaZulu-Natal shelf, SW Indian Ocean, South Africa. Geo-Marine Letters 27, 399-409. https://doi.org/10.1007/s00367-007-0082-2.

Harris, P.T., Whiteway, T., 2011. Global distribution of large submarine canyons: Geomorphic differences between active and passive continental margins. Marine Geology 285, 69-86. https://doi.org/10.1016/j.margeo.2011.05.008.

He, Y., Zhong, G.F., Wang, L.L., Kuang, Z.G., 2014. Characteristics and occurrence of submarine canyon-associated landslides in the middle of the northern continental slope, South China Sea. Marine and Petroleum Geology 57, 546-560. https://doi.org/10.1016/j.marpetgeo.2014.07.003.

Huang, W.K., Qiu, Y., Peng, X.C., Nie, X., Zhuo, H.T., Fu, C.G., 2021. Types and migration of shelf-breaks in the central and eastern parts of the Northern South China Sea and their origin. Marine Geology & Quaternary Geology 41, 1-11 (in Chinese with English abstract). https://doi.org/10.16562/j.cnki.0256-1492.2020060801.

Huang, Z.G, Zhang, W.Q., Cai, F.X., 1995. The submerged Zhujiang Delta. Acta Geographica Sinica 50, 206–214 (in Chinese with English abstract).

Jobe, Z.R., Lowe, D.R., Uchytil, S.J., 2011. Two fundamentally different types of submarine canyons along the continental margin of Equatorial Guinea. Marine and Petroleum Geology 28, 843-860. https://doi.org/10.1016/j.marpetgeo.2010.07.012.

Kneller, B., Dykstra, M., Fairweather, L., Milana, J.P., 2016. Mass-transport and slope accommodation: Implications for turbidite sandstone reservoirs. Aapg Bulletin 100, 213-235. https://doi.org/10.1306/09011514210.

Li, J., Li, W., Alves, T.M., Rebesco, M., Zhan, W., Sun, J., Mitchell, N.C., Wu, S., 2019. Different origins of seafloor undulations in a submarine canyon system, northern South China Sea, based on their seismic character and relative location. Marine Geology 413, 99-111. https://doi.org/10.1016/j.margeo.2019.04.007.

Li, W., Alves, T.M., Rebesco, M., Sun, J., Li, J., Li, S., Wu, S., 2020. The Baiyun Slide Complex, South China Sea: A modern example of slope instability controlling submarine-channel incision on continental slopes. Marine and Petroleum Geology 114, 104231. https://doi.org/10.1016/j.marpetgeo.2020.104231.

Li, W., Wu, S., Voelker, D., Zhao, F., Mi, L., Kopf, A., 2014. Morphology, seismic characterization and sediment dynamics of the Baiyun Slide Complex on the northern South China Sea margin. Journal of the Geological Society 171, 865-877. https://doi.org/10.1144/jgs2014-034.

Li, X.S., Zhou, Q.J., Su, T.Y., Liu, L.J., Gao, S., Zhou, S.W., 2016. Slope-confined submarine canyons in the Baiyun deep-water area, northern South China Sea: variation in their modern morphology. Marine Geophysical Research 37, 95-112. https://doi.org/10.1007/s11001-016-9269-0.

Lin, C., He, M., Steel, R.J., Zhang, Z., Li, H., Zhang, B., Wu, W., Shu, L., Tian, H., Zhang, X., Xing, Z., Wang, S., Zhang, M., 2018. Changes in inner- to outer-shelf delta architecture, Oligocene to Quaternary Pearl River shelf-margin prism, northern South China Sea. Marine Geology 404, 187-204. https://doi.org/10.1016/j.margeo.2018.07.009.

Liu, H.Y., Lin, C.S., Zhang, Z.T., Zhang, B., Jiang, J., Tian, H.X., Liu, H., 2019. High-resolution sequence architecture and depositional evolution of the Quaternary in the northeastern shelf margin of the South China Sea. Acta Oceanologica Sinica 38, 86-98. https://doi.org/10.1007/s13131-019-1442-2.

Lüdmann, T., Kin Wong, H., Wang, P., 2001. Plio–Quaternary sedimentation processes and neotectonics of the northern continental margin of the South China Sea. Marine Geology 172, 331-358. https://doi.org/10.1016/S0025-

3227(00)00129-8.

Ma, B.J., Wu, S.G., Sun, Q.L., Mi, L.J., Wang, Z.Z., Tian, J., 2015. The late Cenozoic deep-water channel system in the Baiyun Sag, Pearl River Mouth Basin: Development and tectonic effects. Deep Sea Research Part II: Topical Studies in Oceanography 122, 226-239. https://doi.org/10.1016/j.dsr2.2015.06.015.

Martin, J., Puig, P., Masque, P., Palanques, A., Sanchez-Gomez, A., 2014. Impact of Bottom Trawling on Deep-Sea Sediment Properties along the Flanks of a Submarine Canyon. Plos One 9, e104536. https://doi.org/10.1371/journal.pone.0104536.

Mayall, M., Jones, E., Casey, M., 2006. Turbidite channel reservoirs-Key elements in facies prediction and effective development. Marine and Petroleum Geology 23, 821-841. https://doi.org/10.1016/j.marpetgeo.2006.08.001.

McAdoo, B.G., 2000. Mapping submarine slope failures. In: Marine and Coastal Geographical Information Systems. Taylor and Francis, London, pp. 189-204.

McHargue, T.R., Webb, J.E., 1986. Internal geometry, seismic facies, and petroleum potential of canyons and inner fan channels of the Indus Submarine Fan. Aapg Bulletin-American Association of Petroleum Geologists 70, 161–180. https://doi.org/10.1306/94885651-1704-11D7-8645000102C1865D.

Mitchell, N.C., 2005. Interpreting long-profiles of canyons in the USA Atlantic continental slope. Marine Geology 214, 75-99. https://doi.org/10.1016/j.margeo.2004.09.005.

Mitchell, N.C., 2008. Summary of progress in geomorphologic modelling of continental slope canyons. Geological Society, London, Special Publications 296, 183-194. https://doi.org/10.1144/sp296.12.

Mountjoy, J.J., Barnes, P.M., Pettinga, J.R., 2009. Morphostructure and evolution of submarine canyons across an active margin: Cook Strait sector of the Hikurangi Margin, New Zealand. Marine Geology 260, 45-68. https://doi.org/10.1016/j.margeo.2009.01.006.

Mulder, T., Ducassou, E., Gillet, H., Hanquiez, V., Tournadour, E., Combes, J., Eberli, G.P., Kindler, P., Gonthier, E., Conesa, G., Robin, C., Sianipar, R., Reijmer, J.J.G., Francois, A., 2012. Canyon morphology on a modern carbonate slope of the Bahamas: Evidence of regional tectonic tilting. Geology 40, 771-774. https://doi.org/10.1130/g33327.1.

Naranjo-Vesga, J., Paniagua-Arroyave, J.F., Ortiz-Karpf, A., Jobe, Z., Wood, L., Galindo, P., Shumaker, L., Mateus-Tarazona, D., 2022. Controls on submarine canyon morphology along a convergent tectonic margin. The Southern Caribbean of Colombia. Marine and Petroleum Geology 137, 105493. https://doi.org/10.1016/j.marpetgeo.2021.105493.

Normandeau, A., Lajeunesse, P., Ghienne, J.-F., Dietrich, P., 2022. Detailed Seafloor Imagery of Turbidity Current Bedforms Reveals New Insight Into Fine-Scale Near-Bed Processes. Geophysical Research Letters 49, e2021GL097389. https://doi.org/10.1029/2021GL097389.

Orange, D.L., 1999. Tectonics, sedimentation, and erosion in northern California: submarine geomorphology and sediment preservation potential as a result of three competing processes. Marine Geology 154, 369-382. https://doi.org/10.1016/S0025-3227(98)00124-8.

Pang, X., Chen, C.M., Zhu, M., He, M., Shen, J., Lian, S.Y., Wu, X.J., Shao, L., 2009. Baiyun Movement: A Significant Tectonic Event on Oligocene/Miocene Boundary in the Northern South China Sea and Its Regional Implications. Journal of Earth Science 20, 49-56. https://doi.org/10.1007/s12583-009-0005-4.

Parsons, J.D., Friedrichs, C.T., Traykovski, P.A., Mohrig, D., Imran, J., Syvitski, J.P.M., Parker, G., Puig, P., Buttles, J.L., Garcia, M.H., 2007. The mechanics of marine sediment gravity flows, in: Nittrouer, C.A., Austin, J.A., Field, M.E., Kravitz, J.H., Syvitski, J.P.M., Wiberg, P.L. (Eds.), Continental Margin Sedimentation: From Sediment Transport to Sequence Stratigraphy. Wiley-Blackwell, Hoboken, pp. 275-337. https://doi.org/10.1002/9781444304398.ch6.

Patruno, S., Hampson, G.J., Jackson, C.A.L., 2015. Quantitative characterisation of deltaic and subaqueous clinoforms. Earth-Science Reviews 142, 79-119. https://doi.org/10.1016/j.earscirev.2015.01.004.

Pope, E.L., Normandeau, A., Ó Cofaigh, C., Stokes, C.R., Talling, P.J., 2019. Controls on the formation of turbidity current channels associated with marine-terminating glaciers and ice sheets. Marine Geology 415, 105951. https://doi.org/10.1016/j.margeo.2019.05.010.

Popescu, I., Lericolais, G., Panin, N., Normand, A., Dinu, C., Le Drezen, E., 2004. The Danube submarine canyon (Black Sea): morphology and sedimentary processes. Marine Geology 206, 249-265. https://doi.org/10.1016/j.margeo.2004.03.003.

Puga-Bernabéu, Á., Webster, J.M., Beaman, R.J., Guilbaud, V., 2013. Variation in canyon morphology on the Great Barrier Reef margin, north-eastern Australia: The influence of slope and barrier reefs. Geomorphology 191, 35-50. https://doi.org/10.1016/j.geomorph.2013.03.001.

Puig, P., Durán, R., Muñoz, A., Elvira, E., Guillén, J., 2017. Submarine canyon-head morphologies and inferred sediment transport processes in the Alías-Almanzora canyon system (SW Mediterranean): On the role of the sediment supply. Marine Geology 393, 21-34. https://doi.org/10.1016/j.margeo.2017.02.009.

Puig, P., Greenan, B.J.W., Li, M.Z., Prescott, R.H., Piper, D.J.W., 2013. Sediment transport processes at the head of Halibut Canyon, eastern Canada margin: An interplay between internal tides and dense shelf-water cascading. Marine Geology 341, 14-28. https://doi.org/10.1016/j.margeo.2013.05.004.

Puig, P., Palanques, A., Martin, J., 2014. Contemporary Sediment-Transport Processes in Submarine Canyons, in: Carlson, C.A., Giovannoni, S.J. (Eds.), Annual Review of Marine Science, Vol 6. Annual Reviews, Palo Alto, pp. 53-77. https://doi.org/10.1146/annurev-marine-010213-135037.

Qin, Yongpeng, Alves, Tiago M., Constantine, José, Gamboa, D., 2017. The Role of Mass Wasting In the Progressive Development Of Submarine Channels (Espírito Santo Basin, Se Brazil). Journal of Sedimentary Research 87, 500-516. https://doi.org/10.2110/jsr.2017.18.

Rebesco, M., Neagu, R.C., Cuppari, A., Muto, F., Accettella, D., Dominici, R., Cova, A., Romano, C., Caburlotto, A., 2009. Morphobathymetric analysis and evidence of submarine mass movements in the western Gulf of Taranto (Calabria margin, Ionian Sea). International Journal of Earth Sciences 98, 791-805. https://doi.org/10.1007/s00531-

009-0429-1.

Shepard, F.P., 1981. Submarine Canyons: Multiple Causes and Long-Time Persistence. Aapg Bulletin-American Association of Petroleum Geologists 65, 1062-1077. https://doi.org/10.1306/03B59459-16D1-11D7-8645000102C1865D.

Shumaker, L.E., Jobe, Z.R., Graham, S.A., 2017. Evolution of submarine gullies on a prograding slope: Insights from 3D seismic reflection data. Marine Geology 393, 35-46. https://doi.org/10.1016/j.margeo.2016.06.006.

Shumaker, L.E., Jobe, Z.R., Johnstone, S.A., Pettinga, L.A., Cai, D., Moody, J.D., 2018. Controls on submarine channel-modifying processes identified through morphometric scaling relationships. Geosphere 14, 2171-2187. https://doi.org/10.1130/ges01674.1.

Su, M., Alves, T.M., Li, W., Sha, Z., Hsiung, K.-H., Liang, J., Kuang, Z., Wu, N., Zhang, B., Chiang, C.-S., 2019. Reassessing two contrasting Late Miocene-Holocene stratigraphic frameworks for the Pearl River Mouth Basin, northern South China Sea. Marine and Petroleum Geology 102, 899-913. https://doi.org/10.1016/j.marpetgeo.2018.12.034.

Su, M., Lin, Z., Wang, C., Kuang, Z., Liang, J., Chen, H., Liu, S., Zhang, B., Luo, K., Huang, S., Wu, Q., 2020. Geomorphologic and infilling characteristics of the slope-confined submarine canyons in the Pearl River Mouth Basin, northern South China Sea. Marine Geology 424, 106166. https://doi.org/10.1016/j.margeo.2020.106166.

Taylor, B., Hayes, D.E., 1980. The tectonic evolution of the South China Basin. Tectonic and Geologic Evolution of Southeast Asian Seas and Islands 23, 89-104. https://doi.org/10.1029/GM023p0089.

Tournadour, E., Mulder, T., Borgomano, J., Gillet, H., Chabaud, L., Ducassou, E., Hanquiez, V., Etienne, S., 2017. Submarine canyon morphologies and evolution in modern carbonate settings: The northern slope of Little Bahama Bank, Bahamas. Marine Geology 391, 76-97. https://doi.org/10.1016/j.margeo.2017.07.014.

Voigt, I., Henrich, R., Preu, B.M., Piola, A.R., Hanebuth, T.J.J., Schwenk, T., Chiessi, C.M., 2013. A submarine canyon as a climate archive — Interaction of the Antarctic Intermediate Water with the Mar del Plata Canyon

(Southwest Atlantic). Marine Geology 341, 46-57. https://doi.org/10.1016/j.margeo.2013.05.002.

Wang, X., Kneller, B., Wang, Y., Chen, W., 2020. Along-strike Quaternary morphological variation of the Baiyun Sag, South China Sea: The interplay between deltas, pre-existing morphology, and oceanographic processes. Marine and Petroleum Geology 122, 104640. https://doi.org/10.1016/j.marpetgeo.2020.104640.

Wang, X., Zhuo, H., Wang, Y., Mao, P., He, M., Chen, W., Zhou, J., Gao, S., Wang, M., 2018. Controls of contour currents on intra-canyon mixed sedimentary processes: Insights from the Pearl River Canyon, northern South China Sea. Marine Geology 406, 193-213. https://doi.org/10.1016/j.margeo.2018.09.016.

Wang, X., Wang, Y., He, M., Chen, W., Zhuo, H., Gao, S., Wang, M., Zhou, J., 2017. Genesis and evolution of the mass transport deposits in the middle segment of the Pearl River canyon, South China Sea: Insights from 3D seismic data. Marine and Petroleum Geology 88, 555-574. https://doi.org/10.1016/j.marpetgeo.2017.08.036.

Wiles, E., Green, A., Watkeys, M., Botes, R., Jokat, W., 2019. Submarine canyons of NW Madagascar: A first geomorphological insight. Deep Sea Research Part II: Topical Studies in Oceanography 161, 5-15. https://doi.org/10.1016/j.dsr2.2018.06.003.

Wu, S., Gao, J., Zhao, S., Luedmann, T., Chen, D., Spence, G., 2014. Post-rift uplift and focused fluid flow in the passive margin of northern South China Sea. Tectonophysics 615, 27-39. https://doi.org/10.1016/j.tecto.2013.12.013.

Yin, S., Lin, L., Pope, E.L., Li, J., Ding, W., Wu, Z., Ding, W., Gao, J., Zhao, D., 2019. Continental slope-confined canyons in the Pearl River Mouth Basin in the South China Sea dominated by erosion, 2004–2018. Geomorphology 344, 60-74. https://doi.org/10.1016/j.geomorph.2019.07.016.

Yu, H., Shing, 1994. Structure, stratigraphy and basin subsidence of tertiary basins along the Chinese southeastern continental margin. Tectonophysics 235, 63-76. https://doi.org/10.1016/0040-1951(94)90017-5.

Zhang, G.X., Chen, F., Yang, S.X., Su, X., Sha, Z.B., Wang, H.B., Liang, J.Q., Zhou, Y., 2012. Accumulation and exploration of gas hydrate in deep-sea sediments of northern South China Sea. Chinese Journal of Oceanology and

Limnology 30, 876-888. https://doi.org/10.1007/s00343-012-1313-6.

Zhong, G., Peng, X., 2021. Transport and accumulation of plastic litter in submarine canyons—The role of gravity flows. Geology 49, 581-586. https://doi.org/10.1130/g48536.1.

Zhou, W., Chiarella, D., Zhuo, H., Wang, Y., Tang, W., Zou, M., Xu, Q., 2021. Genesis and evolution of large-scale sediment waves in submarine canyons since the Penultimate Glacial Maximum (ca. 140 ka), northern South China Sea margin. Marine and Petroleum Geology 134, 105381. https://doi.org/10.1016/j.marpetgeo.2021.105381.

Zhou, W., Wang, Y., Gao, X., Zhu, W., Xu, Q., Xu, S., Cao, J., Wu, J., 2015. Architecture, evolution history and controlling factors of the Baiyun submarine canyon system from the middle Miocene to Quaternary in the Pearl River Mouth Basin, northern South China Sea. Marine and Petroleum Geology 67, 389-407. https://doi.org/10.1016/j.marpetgeo.2015.05.015.

Zhu, M.Z., Graham, S., Pang, X., McHargue, T., 2010. Characteristics of migrating submarine canyons from the middle Miocene to present: Implications for paleoceanographic circulation, northern South China Sea. Marine and Petroleum Geology 27, 307-319. https://doi.org/10.1016/j.marpetgeo.2009.05.005.

Zhu, W.L., Huang, B.J., Mi, L.J., Wilkins, R.W.T., Fu, N., Xiao, X.M., 2009. Geochemistry, origin, and deep-water exploration potential of natural gases in the Pearl River Mouth and Qiongdongnan basins, South China Sea. Aapg Bulletin 93, 741-761. https://doi.org/10.1306/02170908099.

Zhuo, H.T., Wang, Y.M., Sun, Z., Wang, Y., Xu, Q., Hou, P.F., Wang, X.X., Zhao, Z.X., Zhou, W., Xu, S., 2019. Along-strike variability in shelf-margin morphology and accretion pattern: An example from the northern margin of the South China Sea. Basin Research 31, 431-460. https://doi.org/10.1111/bre.12329.

Figures

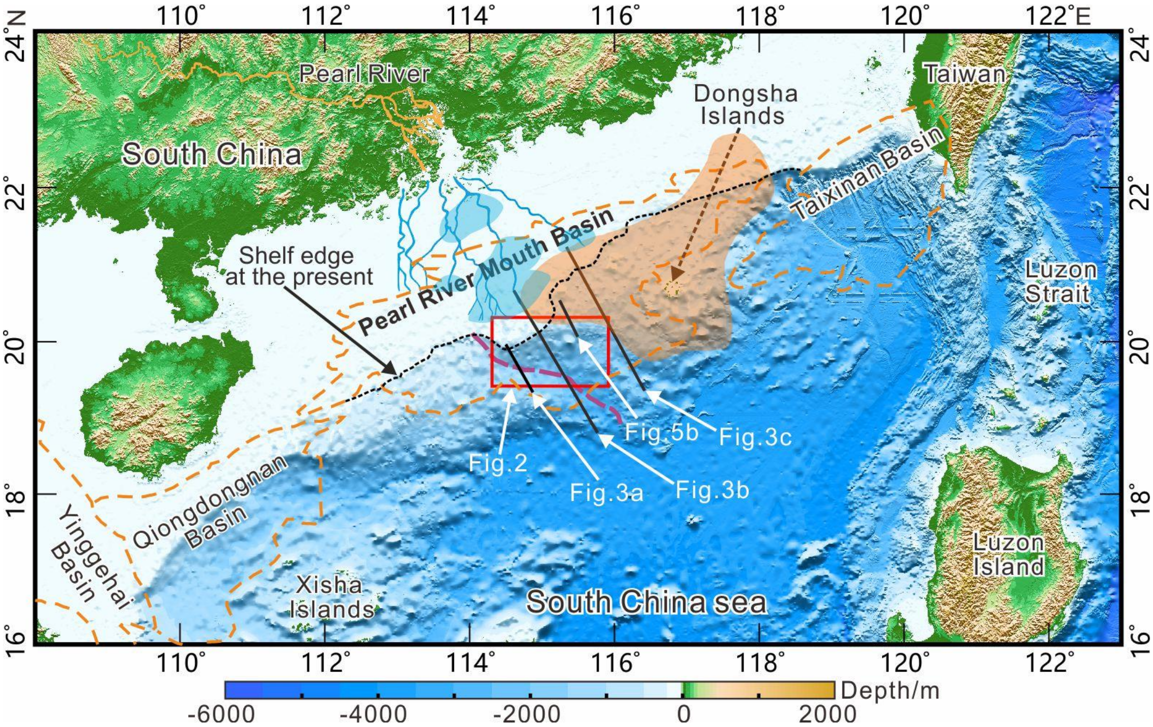

Figure 1

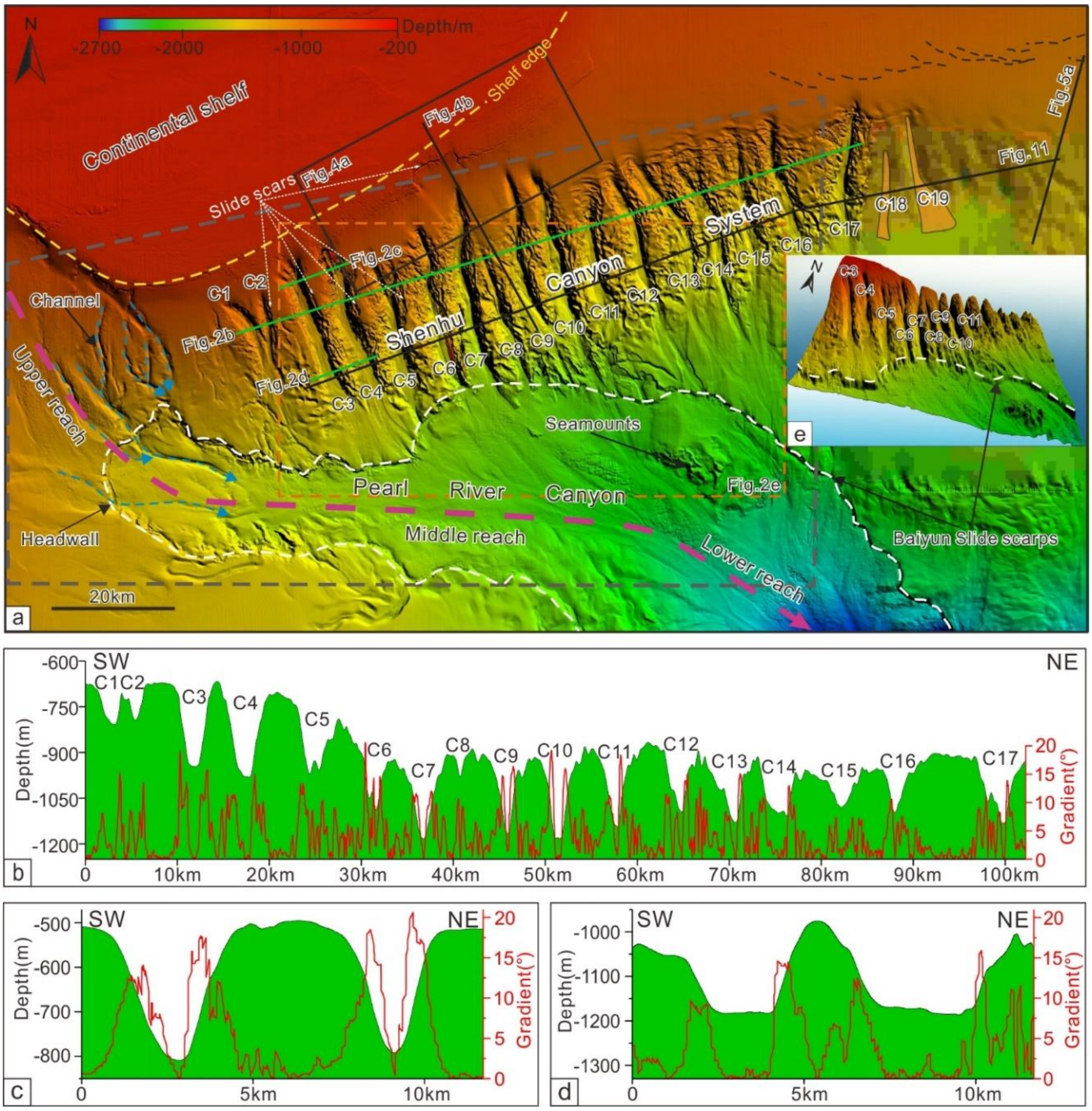
N
Depth/m
-2700 -2000 -1000 -200
Continental shelf
Shelf edge
Fig.4b
Fig.4a
Slide scars
Fig.2c
Fig.2b
Fig.2d
Fig.5a
Fig.11
Fig.2e
Channel
Upper reach
Headwall
Shenhu Canyon System
Pearl River Canyon
Middle reach
Lower reach
Seamounts
Baiyun Slide scarps
C1 C2 C3 C4 C5 C6 C7 C8 C9 C10 C11 C12 C13 C14 C15 C16 C17 C18 C19
20km
a
e
b
SW
NE
Depth(m)
Gradient(°)
0 10km 20km 30km 40km 50km 60km 70km 80km 90km 100km
c
d
5km 10km

Figure 2

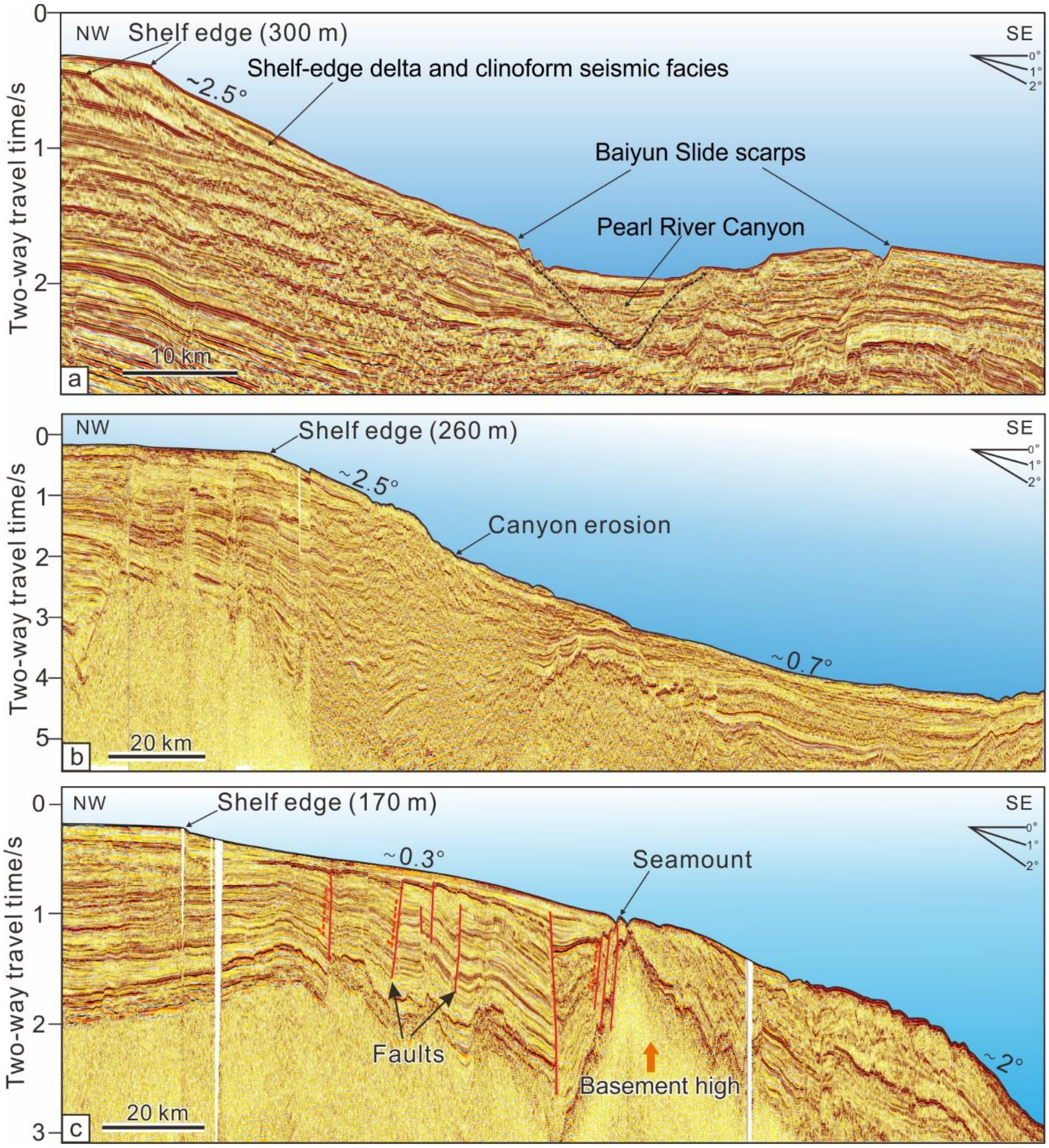

NW
Shelf edge (300 m)
SE
Shelf-edge delta and clinoform seismic facies
~2.5°
Baiyun Slide scarps
Pearl River Canyon
Two-way travel time/s
10 km
a
NW
Shelf edge (260 m)
SE
~2.5°
Canyon erosion
~0.7°
20 km
b
NW
Shelf edge (170 m)
SE
~0.3°
Seamount
Faults
Basement high
~2°
20 km
c

Figure 3

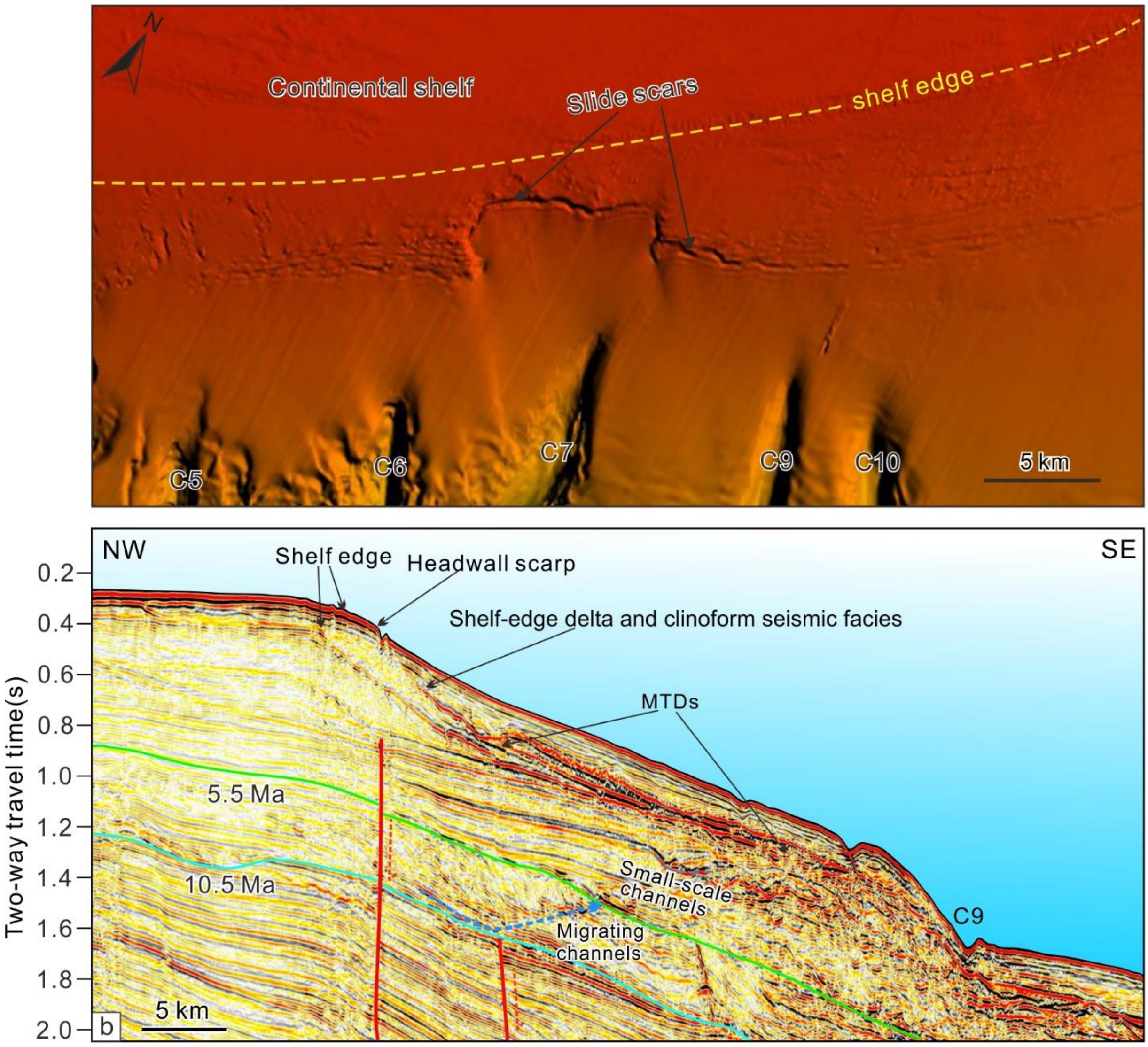
N
Continental shelf
Slide scars
shelf edge
C5
C6
C7
C9
C10
5 km
NW
SE
Shelf edge
Headwall scarp
Shelf-edge delta and clinoform seismic facies
MTDs
5.5 Ma
10.5 Ma
Small-scale channels
Migrating channels
C9
Two-way travel time(s)
0.2
0.4
0.6
0.8
1.0
1.2
1.4
1.6
1.8
2.0
b
5 km

Figure 4

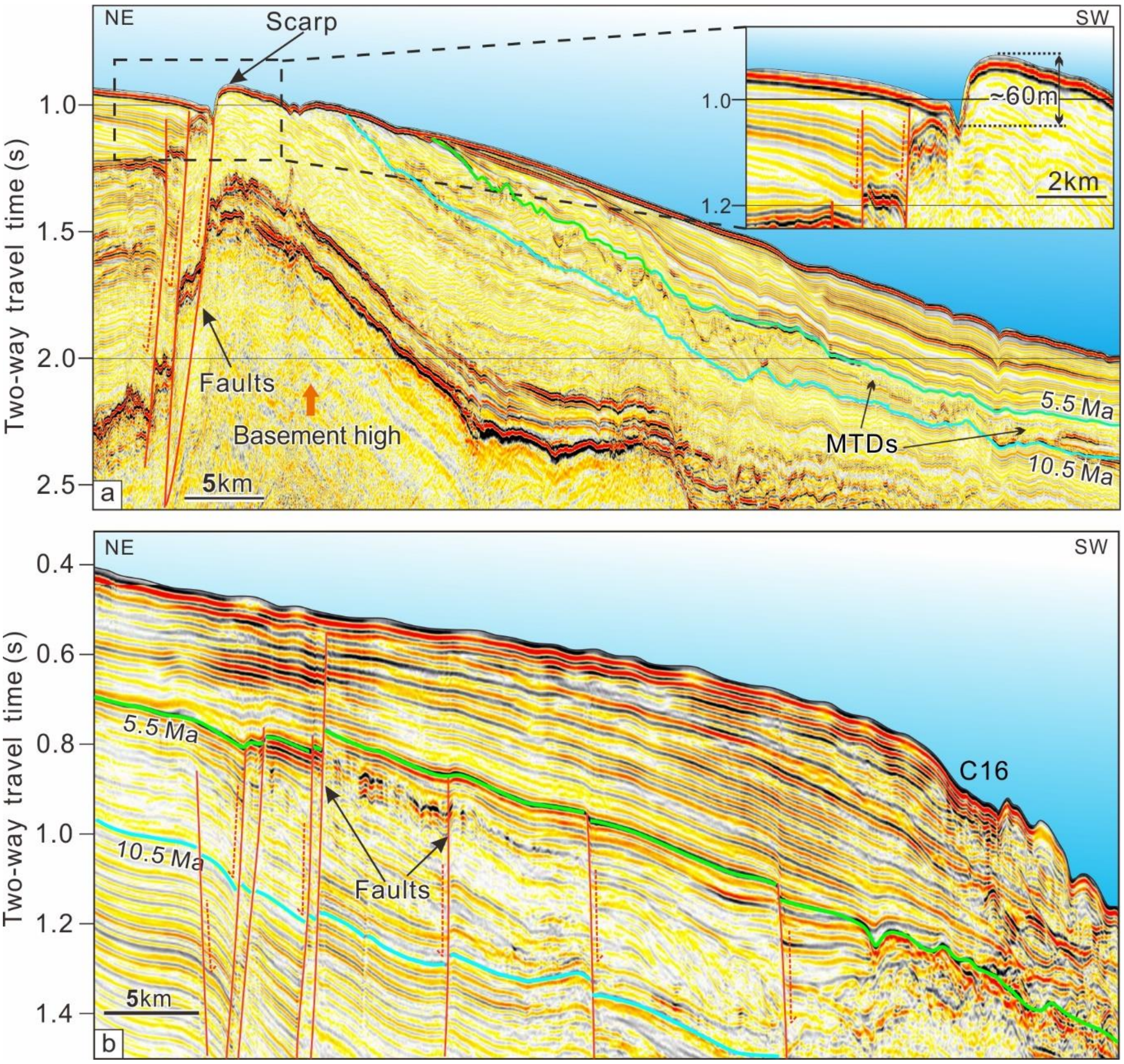

NE
SW
Scarp
~60m
2km
Faults
Basement high
MTDs
5.5 Ma
10.5 Ma
5km
a
Two-way travel time (s)
NE
SW
5.5 Ma
10.5 Ma
Faults
C16
5km
b
Two-way travel time (s)

Figure 5

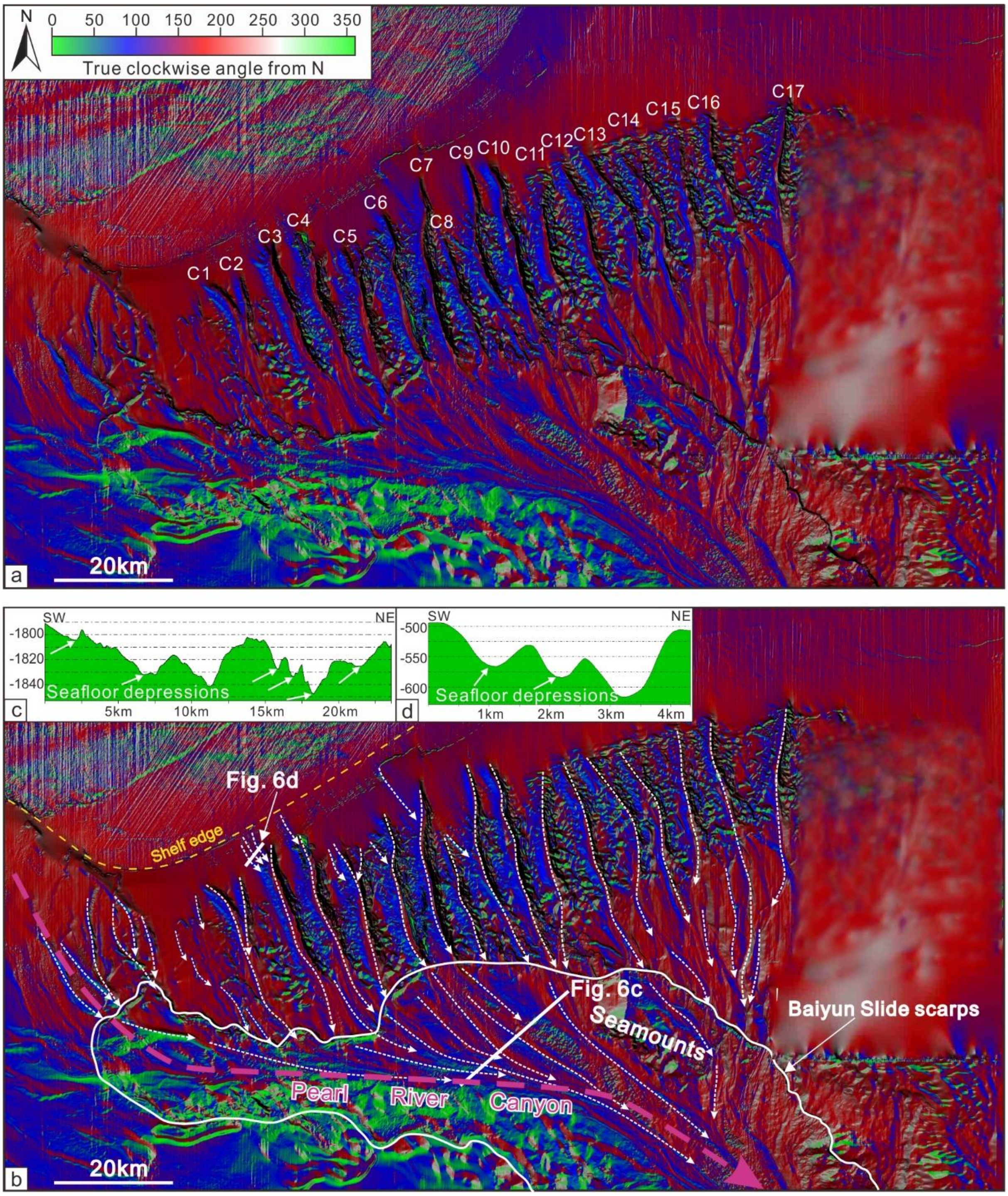

816

817 Figure 6

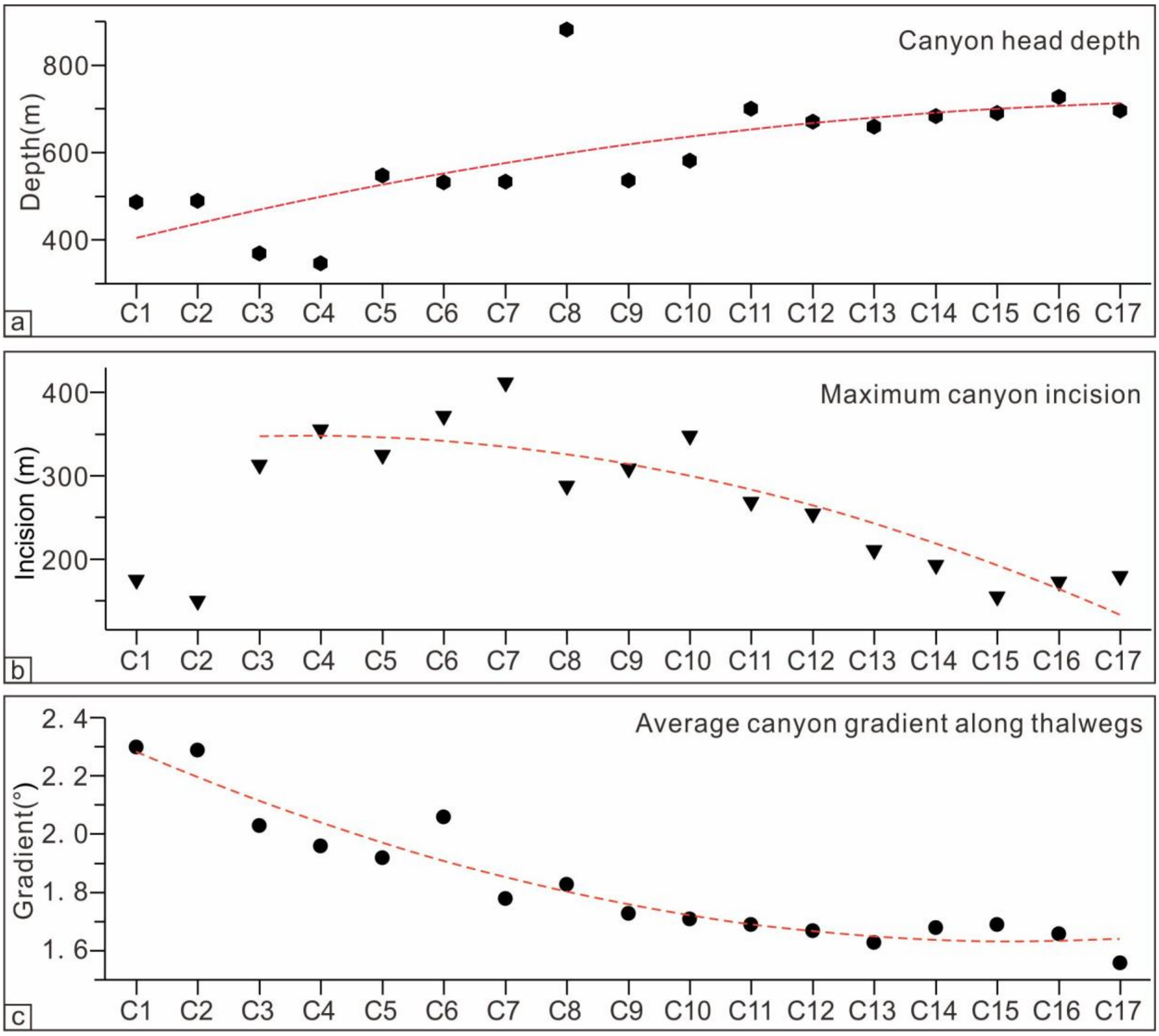
Canyon head depth
Depth(m)
800
600
400
C1 C2 C3 C4 C5 C6 C7 C8 C9 C10 C11 C12 C13 C14 C15 C16 C17
a
Maximum canyon incision
Incision (m)
400
300
200
b
Average canyon gradient along thalwegs
Gradient(°)
2. 4
2. 2
2. 0
1. 8
1. 6
c

Figure 7

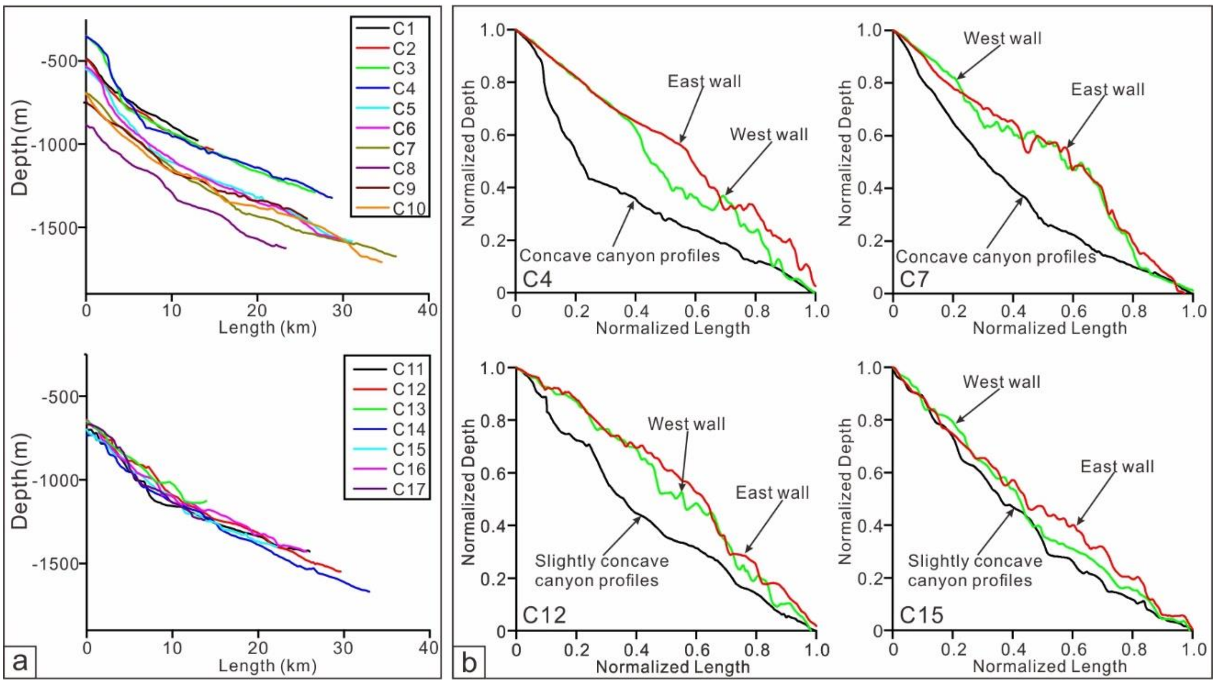
C1
C2
C3
C4
C5
C6
C7
C8
C9
C10
Depth(m)
Length (km)
C11
C12
C13
C14
C15
C16
C17
a
b
Normalized Depth
Normalized Length
East wall
West wall
Concave canyon profiles
C4
C7
C12
C15
Slightly concave canyon profiles

Figure 8

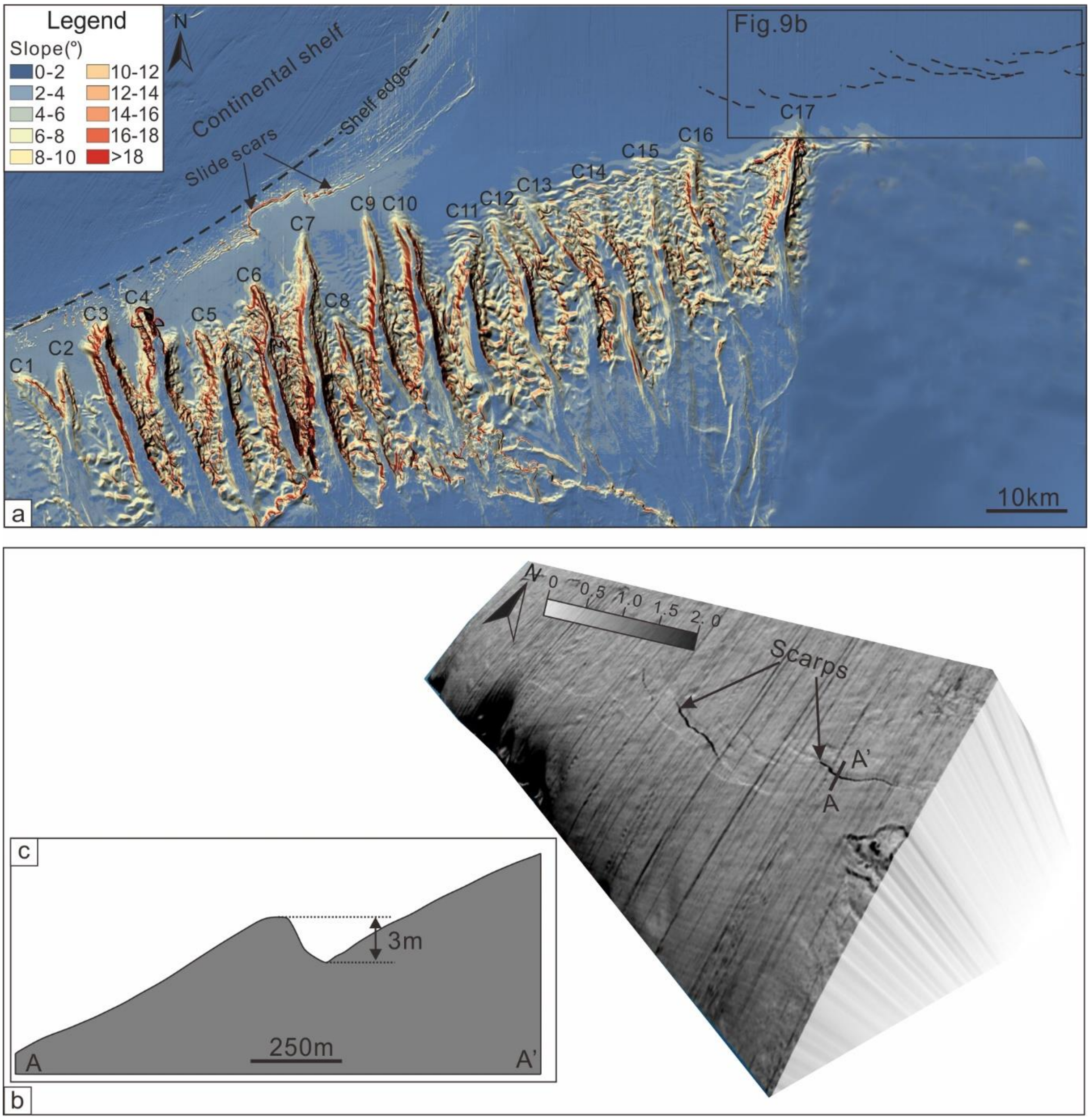
Legend
Slope(°)
0-2
2-4
4-6
6-8
8-10
10-12
12-14
14-16
16-18
>18
N
Continental shelf
Shelf edge
Slide scars
Fig.9b
C1
C2
C3
C4
C5
C6
C7
C8
C9
C10
C11
C12
C13
C14
C15
C16
C17
10km
a
0
0.5
1.0
1.5
2.0
Scarps
A'
A
c
3m
250m
A
A'
b

Figure 9

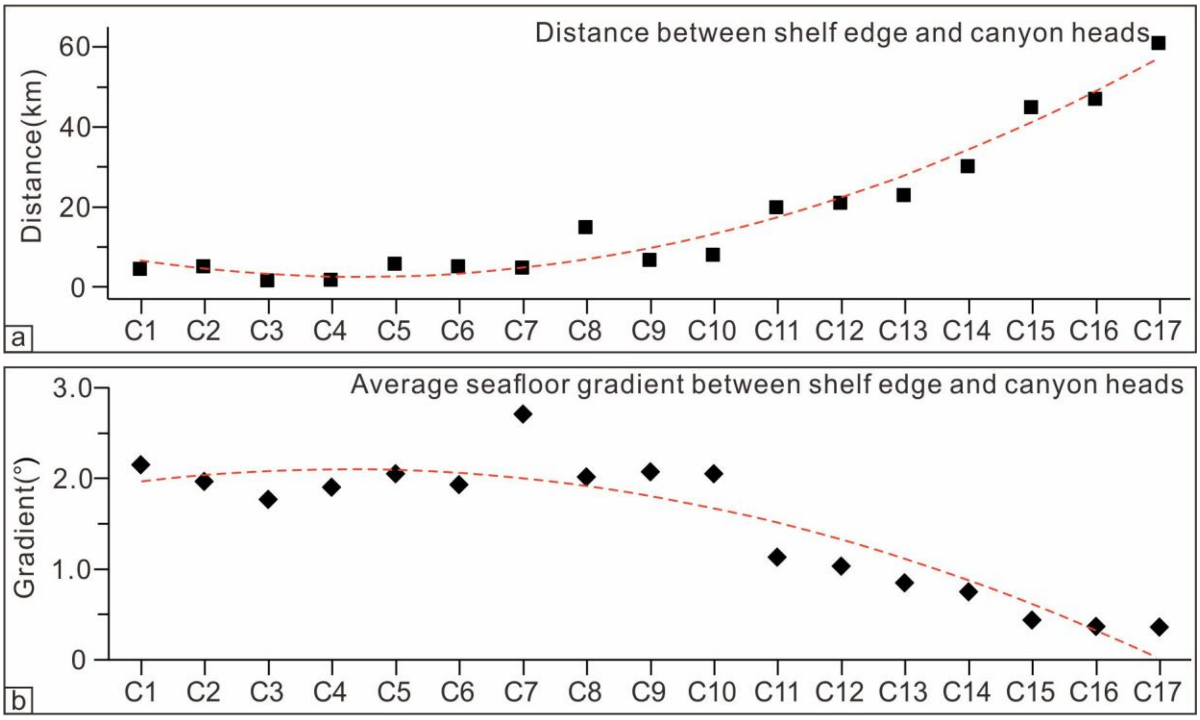
Distance between shelf edge and canyon heads
Distance(km)
60
40
20
0
C1 C2 C3 C4 C5 C6 C7 C8 C9 C10 C11 C12 C13 C14 C15 C16 C17
a
Average seafloor gradient between shelf edge and canyon heads
Gradient(°)
3.0
2.0
1.0
0
C1 C2 C3 C4 C5 C6 C7 C8 C9 C10 C11 C12 C13 C14 C15 C16 C17
b

Figure 10

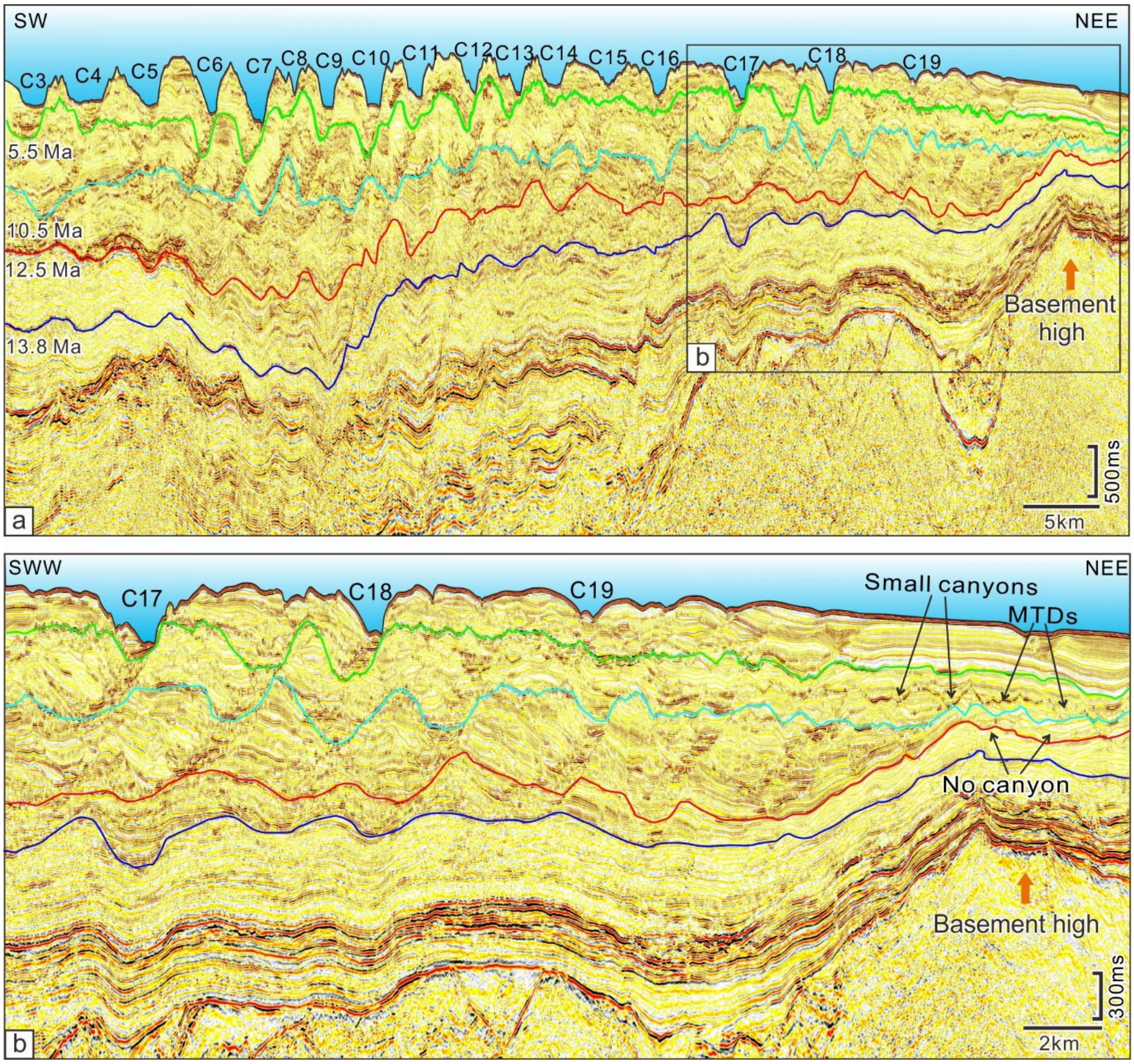
SW
NEE
C3
C4
C5
C6
C7
C8
C9
C10
C11
C12
C13
C14
C15
C16
C17
C18
C19
5.5 Ma
10.5 Ma
12.5 Ma
13.8 Ma
Basement high
b
500ms
5km
a
SWW
NEE
C17
C18
C19
Small canyons
MTDs
No canyon
Basement high
300ms
2km
b

Figure 11

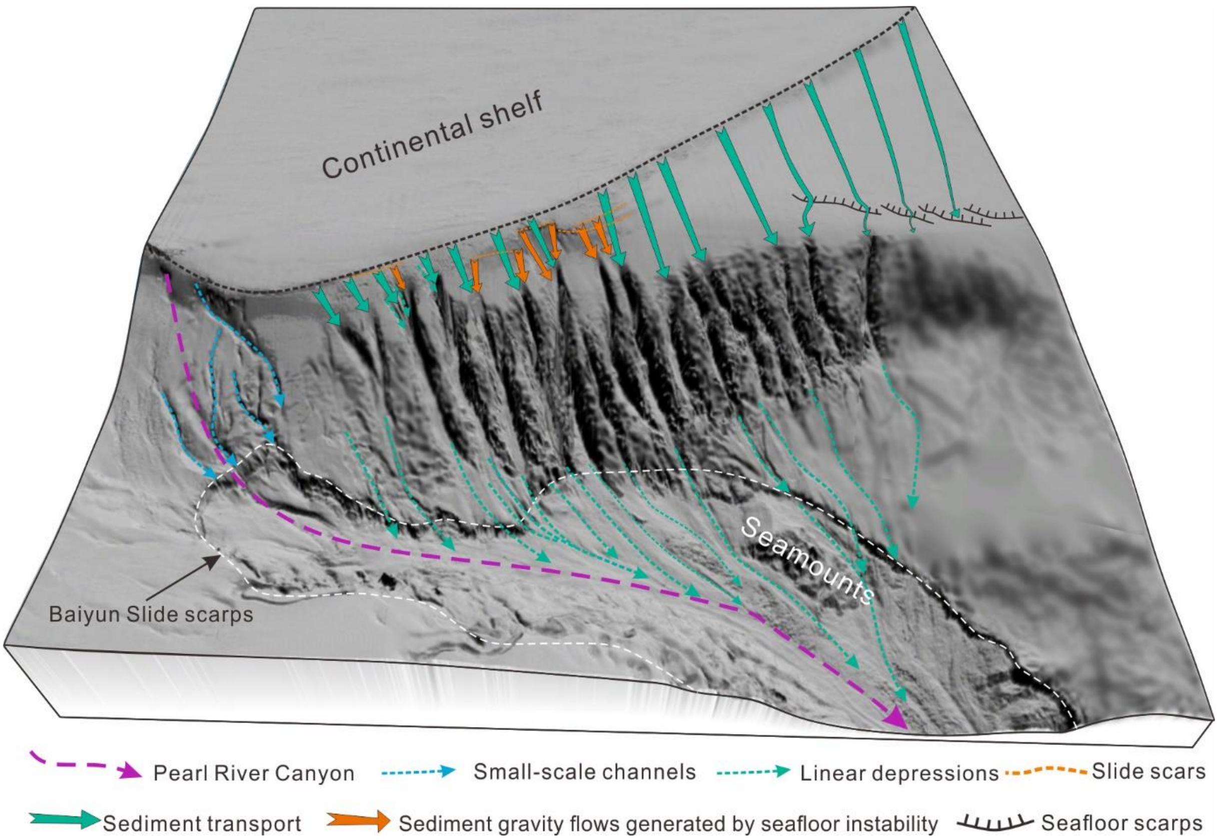
Continental shelf
Seamounts
Baiyun Slide scarps
Pearl River Canyon
Small-scale channels
Linear depressions
Slide scars
Sediment transport
Sediment gravity flows generated by seafloor instability
Seafloor scarps

Figure 12

Table

C	HD (m)	TD (m)	L (km)	SL (km)	S	MI (m)	CGr (°)	Az	D (km)	SGr (°)
1	487	977	13.0	12.2	1.06	175	2.30	144	4.5	2.15
2	490	1050	14.8	12.7	1.17	150	2.29	169	5.1	1.97
3	370	1290	26.7	26.5	1.01	313	2.03	157	1.6	1.77
4	350	1323	28.7	28.5	1.01	356	1.96	157	1.8	1.90
5	547	1583	31.0	30.8	1.01	325	1.92	162	5.8	2.05
6	532	1575	29.9	29.0	1.03	372	2.06	161	5.1	1.93
7	533	1675	36.2	35.3	1.03	412	1.78	164	4.9	2.71
8	880	1626	23.4	23.2	1.01	288	1.83	160	15.0	2.02
9	536	1450	25.9	25.4	1.02	309	1.73	163	6.8	2.07
10	582	1453	26.2	25.8	1.02	348	1.71	168	8.0	2.05
11	700	1550	29.5	29.2	1.01	270	1.69	158	20.0	1.13
12	671	1401	26.7	25.8	1.03	255	1.67	153	21.0	1.03
13	660	1669	33.5	33.1	1.01	211	1.63	159	23.0	0.85
14	683	1402	22.5	22.3	1.01	193	1.68	169	30.2	0.75
15	691	1429	25.5	25.1	1.01	155	1.69	166	45.0	0.44
16	730	1428	23.8	23.4	1.02	173	1.66	161	47.0	0.37
17	696	1413	22.5	22.3	1.01	180	1.56	180	61.0	0.36

Table 1